

Anterior cingulate cortex parvalbumin and somatostatin interneurons shape social behavior in male mice

Received: 25 January 2024

Accepted: 22 April 2025

Published online: 04 May 2025



Chuchu Qi^{1,4}, Wenqi Sima^{1,4}, Honghui Mao^{1,4}, Erling Hu¹, Junye Ge¹,
Mao Deng², Andi Chen¹, Weiyi Ye², Qian Xue¹, Wenting Wang^{1,3}✉,
Qian Chen²✉ & Shengxi Wu¹✉

The anterior cingulate cortex (ACC) is essential for social behavior, and its dysfunction is implicated in social interaction deficits in autism. Pyramidal neuron activity in the ACC is modulated by parvalbumin (PV) and somatostatin (SST) interneurons, though their specific roles in social interactions remain unclear. Here, we demonstrate that PV and SST interneurons differentially contribute to the regulation of social interactions. In a *Shank3*-deficient autistic model, the expression of *Kcnh7*, a risk gene for autism, is reduced in both PV and SST interneurons. Knocking out *Kcnh7* in either interneuron subtype leads to social interaction deficits. Furthermore, projections from the lateral posterior thalamic nucleus (mediorostral part, LPMR) to PV interneurons and from the ventral hippocampus (vHPC) to SST interneurons differentially modulate social interactions. These findings provide new insights into the distinct roles of PV and SST interneurons in social processes and their contributions to autism-related pathophysiology.

Social behavior comprises interaction, hierarchy, anxiety, courtship, and parenting, all of which are crucial for population survival and longevity. Among these, social interactions are particularly significant, serving as the foundation for other behaviors by facilitating information exchange and regulating sociability (identifying unfamiliar individuals) and preference (distinguishing between unfamiliar and familiar individuals)¹. Considering the importance of social interaction, animal models are essential for investigating the neural mechanisms and brain regions involved in social behaviors and disorders such as autism spectrum disorder (ASD)². The three-chamber test is widely used assay to evaluate social behaviors across species, including mice, dogs, and zebrafish^{3–5}. In the first phase, the animal explores a central chamber and two adjacent chambers—one containing an unfamiliar conspecific and the other empty—to evaluate sociability. In the second phase, social preference is evaluated by differentiating between unfamiliar and familiar individuals. This task highlights the

evolutionary conservation of fundamental social interaction mechanisms across species^{1,6}.

The anterior cingulate cortex (ACC) is a key region implicated in social abnormalities, particularly in *Shank3* mutant ASD models. *Shank3* encodes postsynaptic scaffolding proteins at excitatory synapses, and its mutations are strongly associated with ASD^{7,8}. Imaging studies have linked ACC neural activity to variations in social behavior in humans and nonhuman primates^{9,10}, while structural and functional changes in the ACC correlate with social deficits in autism^{11,12}. However, the precise mechanisms of ACC in regulating social interaction remain relatively understudied.

The ACC consists of both excitatory pyramidal neurons and GABAergic interneurons¹³. Among the latter, parvalbumin (PV) and somatostatin (SST) interneurons play a critical role in regulating cortical function by fine-tuning pyramidal neuron activity^{14–17}. These interneurons differentially modulate pyramidal neuron dynamics and

¹Department of Neurobiology, School of Basic Medicine, Fourth Military Medical University, Xi'an, Shaanxi, China. ²Zhongshan Institute for Drug Discovery, Shanghai Institute of Materia Medica, Chinese Academy of Sciences, Zhongshan, China. ³Innovation Research Institute, Xijing Hospital, Fourth Military Medical University, Xi'an, China. ⁴These authors contributed equally: Chuchu Qi, Wenqi Sima, Honghui Mao. ✉e-mail: wwt0657@fmmu.edu.cn; chenqian@zidd.ac.cn; shengxi@fmmu.edu.cn

stabilize network output through distinct intrinsic properties and synaptic input profiles¹⁸. Given their distinct functions, PV and SST interneurons may differentially influence ACC microcircuits, potentially impacting social interactions and contributing to social deficits in ASD. Notably, social deficits, a core symptom of ASD, exhibit high heterogeneity^{19–21}, complicating both the diagnosis and treatment of ASD patients. If PV and SST interneurons indeed selectively modulate ACC-related social processes, it is worth investigating whether they contribute to the heterogeneity of social deficits and exploring the underlying mechanisms.

In this study, we found that PV and SST interneurons in the ACC contribute to the different phases of social interaction. Notably, in *Shank3* mutant mice, we detected reduced expression of *Kcnh7*, which encodes potassium voltage-gated channel subfamily H (eag-related, Kv11.3), in both PV interneurons and SST interneurons. *Kcnh7* is also recognized as a risk gene for ASD²², and previous studies have shown that Kv11.3 regulates the resting membrane potential and action potential firing in neurons²³. Using a Cre-dependent CRISPR-Cas9 viral approach to knockout *Kcnh7* in PV or SST interneurons in the ACC, we found that PV interneurons primarily regulate sociability, whereas SST interneurons influence both sociability and social preference. The distinct contributions of PV and SST interneurons are partially due to their differential inputs. These findings provide direct evidence for the specific roles of ACC PV and SST interneurons in social interaction and offer insights into the potential mechanisms underlying social dysfunction in individuals with ASD.

Results

PV and SST interneuron activity in the ACC differentially reduces during distinct phases of social interaction

Initially, we aimed to investigate the involvement of PV and SST interneurons in modulating social behavior during the home cage test. To this end, we employed in vivo fiber photometry to monitor the dynamics of PV and SST interneurons during social interactions by injecting an adeno-associated virus (AAV), AAV2/9-FLEX-GCaMP7s, into the ACC of PV-Cre or SST-Cre mice (Fig. 1a–c and Supplementary Fig. 1a, b)^{14,24}. In the test, an unfamiliar juvenile mouse was introduced into the subject mouse's enclosure. Various types of social interactions between the two mice were recorded, including direct confrontation, olfactory exploration, and chasing (Fig. 1d). We measured bulk calcium signal fluctuations in PV or SST interneurons in the ACC during these behavioral events, with the zero-point defined as the moment the subject mouse's nose or forelimbs contacted the juvenile stranger. The results showed a significant reduction in PV and SST interneuron activity in response to social stimuli (Fig. 1e, f). Next, we assessed PV and SST interneuron dynamics during sociability and social preference phases using the three-chamber test⁶, defining the calcium signal zero-point as the subject mouse being within a mouse's head length from an unfamiliar mouse's cage. Similar to the home cage test, PV and SST interneurons activity decreased when mice entered social or empty zones, with greater suppression observed in the social zone (Fig. 1g–i and Supplementary Fig. 1c, d, g left, h left). During the social preference phase, activity reduction was more pronounced in the stranger zone than in the original zone (Fig. 1j–l and Supplementary Fig. 1e, f, g middle, h middle). Notably, PV interneuron activity decreased more during sociability with a social partner than during social preference with an unfamiliar mouse (Supplementary Fig. 1g right). In contrast, SST interneuron activity decreased more during social preference with a novel individual than during sociability with a social partner (Supplementary Fig. 1h right). These findings suggest that the activity of PV and SST interneurons is significantly suppressed during social behavior, highlighting their significant roles in social interaction processing.

We compared GCaMP signal dynamics between PV and SST interneurons (Fig. 1m–o). In the home cage test, PV interneurons had

lower area under curve (AUC) values than SST interneurons (Fig. 1m left). Both PV and SST interneurons showed significant correlations between AUC values and social event duration, with a stronger correlation observed in PV interneurons (Fig. 1m right). A similar trend was noted during the sociability phase in the three-chamber test (Fig. 1n). However, during the social preference phase, SST interneurons exhibited greater AUC variation and steeper correlation slopes compared to PV interneurons (Fig. 1o). PV interneuron activity was slightly lower than SST interneuron activity in the original zone (Supplementary Fig. 1i). Overall, in the ACC, PV and SST interneuron activity was suppressed during social interaction, with PV interneuron activity changes being more prominent during sociability and SST interneuron changes being more pronounced during social preference.

Targeted apoptosis of PV and SST interneurons alters the behavior during the two phases of the three-chamber test

We next examined the effect of silencing PV or SST interneurons on social behavior using taCasp3-expressing virus to induce cell-specific apoptosis²⁵ (Fig. 2a, b). Successful ablation of PV and SST interneurons in the ACC was confirmed (Fig. 2c–e). In the three-chamber test, PV-Cre mice maintained a preference for the social zone before and after ablation; however, their discrimination score significantly increased following the intervention (Fig. 2f–h). In contrast, during the social preference phase, ablation of PV neuron eliminated zone preference, with discrimination scores nearing significance (Fig. 2i, j). SST neuron ablation did not affect social zone preference in sociability test (Fig. 2k, l) but significantly increased discrimination scores in the social preference test (Fig. 2m–o). PV-Cre mice exhibited higher discrimination scores than SST-Cre mice following the intervention in sociability test (Supplementary Fig. 2a). Conversely, SST-Cre mice showed a greater preference for the stranger zone in the social preference test after the intervention (Supplementary Fig. 2b). Additionally, PV-Cre mice displayed enhanced social interaction in the home cage test (Supplementary Fig. 2c). These findings demonstrate that PV interneurons may play a more significant role in sociability, whereas SST interneurons are more critical for social preference.

PV interneuron activation reduces sociability more strongly than SST interneuron activation in the home cage test

Given that PV and SST interneurons ablation impaired social behavior in the three-chamber test, we hypothesized that their activation would suppress social interactions. To test this, we used a Cre-dependent strategy to express Channelrhodopsin-2 (ChR2) specifically in ACC PV or SST interneurons (Fig. 3a). ChR2 expression was confirmed in >90% of PV and SST interneurons (Supplementary Fig. 3a, b), with reliable action potential generation at 40 Hz photostimulation (Supplementary Fig. 3c, d), consistent with previous study²⁶. In the home cage test, PV interneuron activation significantly reduced social exploration behaviors, resulting in a decreased frequency and duration of social interactions during laser stimulation (Fig. 3b left). Notably, social interaction time did not fully recover after stimulation in PV-ChR2 mice (Fig. 3b right). Similarly, SST interneuron activation also reduced social events and total interaction time, although partial recovery was observed post-stimulation (Fig. 3c).

To rule out the possibility that the subject mouse became familiar with the stranger mouse over time, we analyzed correlations between interaction times across different stages (OFF1, ON, OFF2). While interaction duration naturally decreased over time in Cre-negative mice, optogenetic stimulation of PV and SST interneurons weakened this correlation, indicating disrupted normal social interaction dynamics (Fig. 3d). PV interneuron activation caused a greater reduction in social events compared to SST activation, as reflected by the social inhibition index (Fig. 3e). When a toy mouse replaced the stranger mouse, both PV-Cre and SST-Cre groups showed similar

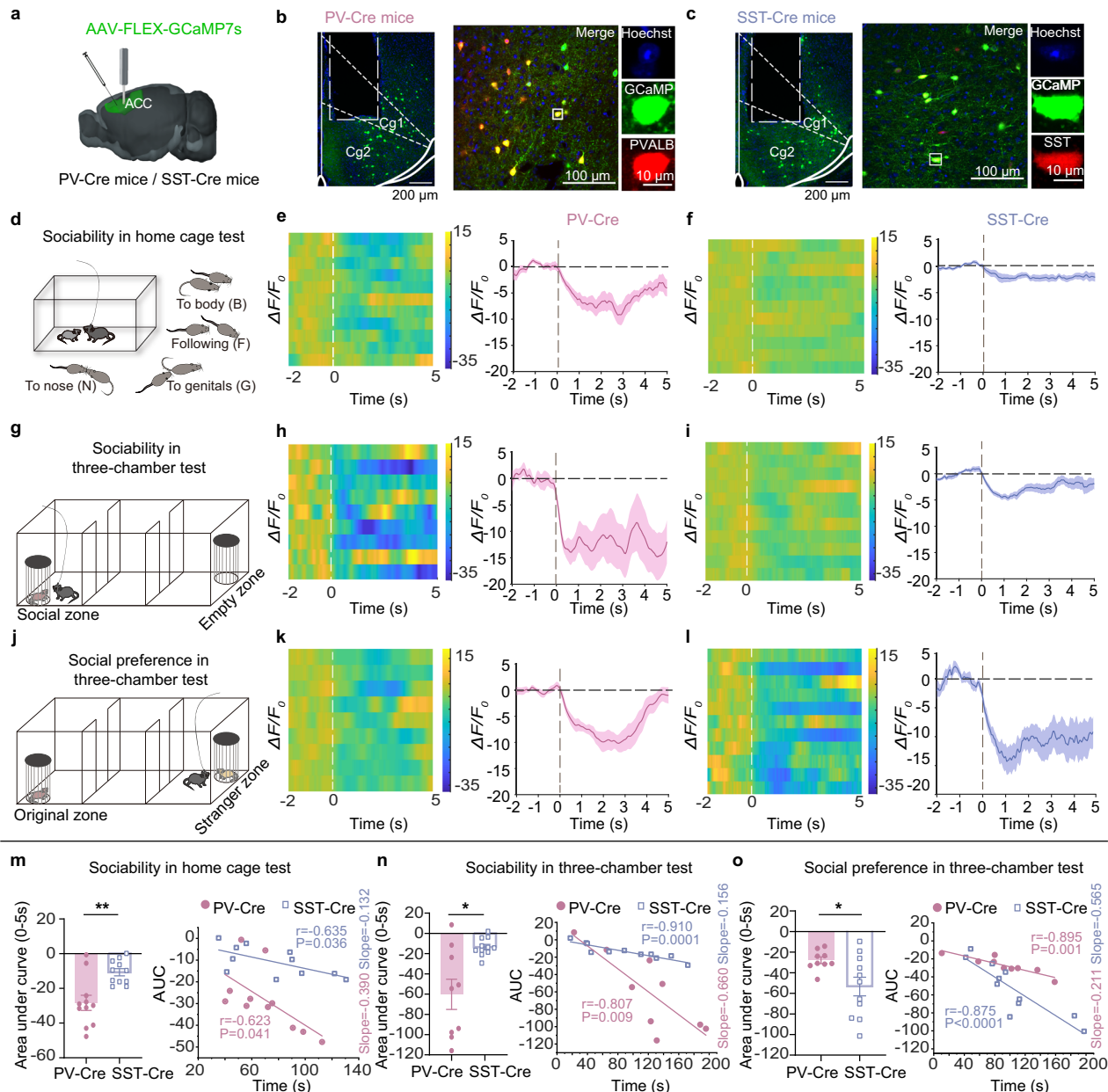


Fig. 1 | The activity of PV and SST interneurons varies during different phases of social interactions. **a** Schematic diagram of AAV-FLEX-GCaMP7s injection (The 3D brain image was created with CEBIT/ION Digital Brain <https://www.digital-brain.cn/>). **b** Example image showing fiber placement in the ACC (left) and GCaMP7s expression (right). **c** Same as **(b)** but for SST-Cre mice. **d** Cartoon depicting the social recognition behavior in the home cage test. **e** Ca^{2+} signals associated with social recognition in **(d)**. Left: heatmap of Ca^{2+} signals, with each row representing one mouse. Right: the peri-event plot of the average Ca^{2+} transients; thick lines indicate the mean, shaded areas represent the SEM ($n = 11$ mice). **f** Same as **(e)** but for SST-Cre mice, $n = 11$ mice. **g** Schematic diagram of the three-chamber sociability test. **h**, **i** Same as **(e)** but for PV-Cre (**h**, $n = 9$ mice) and SST-Cre (**i**, $n = 11$ mice) mice in the sociability test. **j**, **k**, **l** Same as **(g**, **h**, **i**) but for PV-Cre (**k**, $n = 9$ mice) and SST-Cre

(**l**, $n = 11$ mice) mice in social preference test. Schematic diagrams in **(d**, **g**, **j**) are designed by us. **m** Comparison of AUC (area under curve) (left) and the correlation index between social duration and neuronal activity in the PV-Cre and SST-Cre groups (right) ($n = 11$ mice per group, two-tailed unpaired t test, $t = -3.665$, $P = 0.002$; Pearson correlation test, $r = -0.623$, $P = 0.041$ for PV, $r = -0.635$, $P = 0.036$ for SST). **n** Same as **(m)** but for sociability ($n = 9$ PV-Cre mice, $n = 11$ SST-Cre mice, two-tailed unpaired t test, $t = -3.087$, $P = 0.014$; Pearson correlation test, $r = -0.807$, $P = 0.009$ for PV, $r = -0.910$, $P = 0.0001$ for SST). **o** Same as **(m)** but for social preference ($n = 9$ PV-Cre mice, $n = 11$ SST-Cre mice, two-tailed unpaired t test, $t = 2.656$, $P = 0.020$; Pearson correlation test, $r = -0.895$, $P = 0.001$ for PV, $r = -0.875$, $P < 0.0001$ for SST). All statistical tests are two-sided. Data are presented as mean \pm SEM. * $P < 0.05$, ** $P < 0.01$. Source data are provided as a Source Data File.

interaction levels regardless of laser status (Fig. 3f, g). Additionally, PV or SST interneuron activation did not alter preference for stranger mouse urine in an open field (Supplementary Fig. 4). The results indicate that both PV and SST interneurons modulate sociability in the home cage test, with PV interneuron activation exerting a stronger inhibitory effect on social behavior compared to SST interneuron activation.

PV and SST interneuron activation suppresses sociability and social preference in the three-chamber test

To investigate whether optogenetic stimulation of PV and SST interneurons alters social behavior in the three-chamber test, we examined their effects during sociability and social preference stages. In the sociability stage, PV-Cre mice initially exhibited a preference for the unfamiliar mouse (OFF1, Fig. 4a, b left). However, blue light

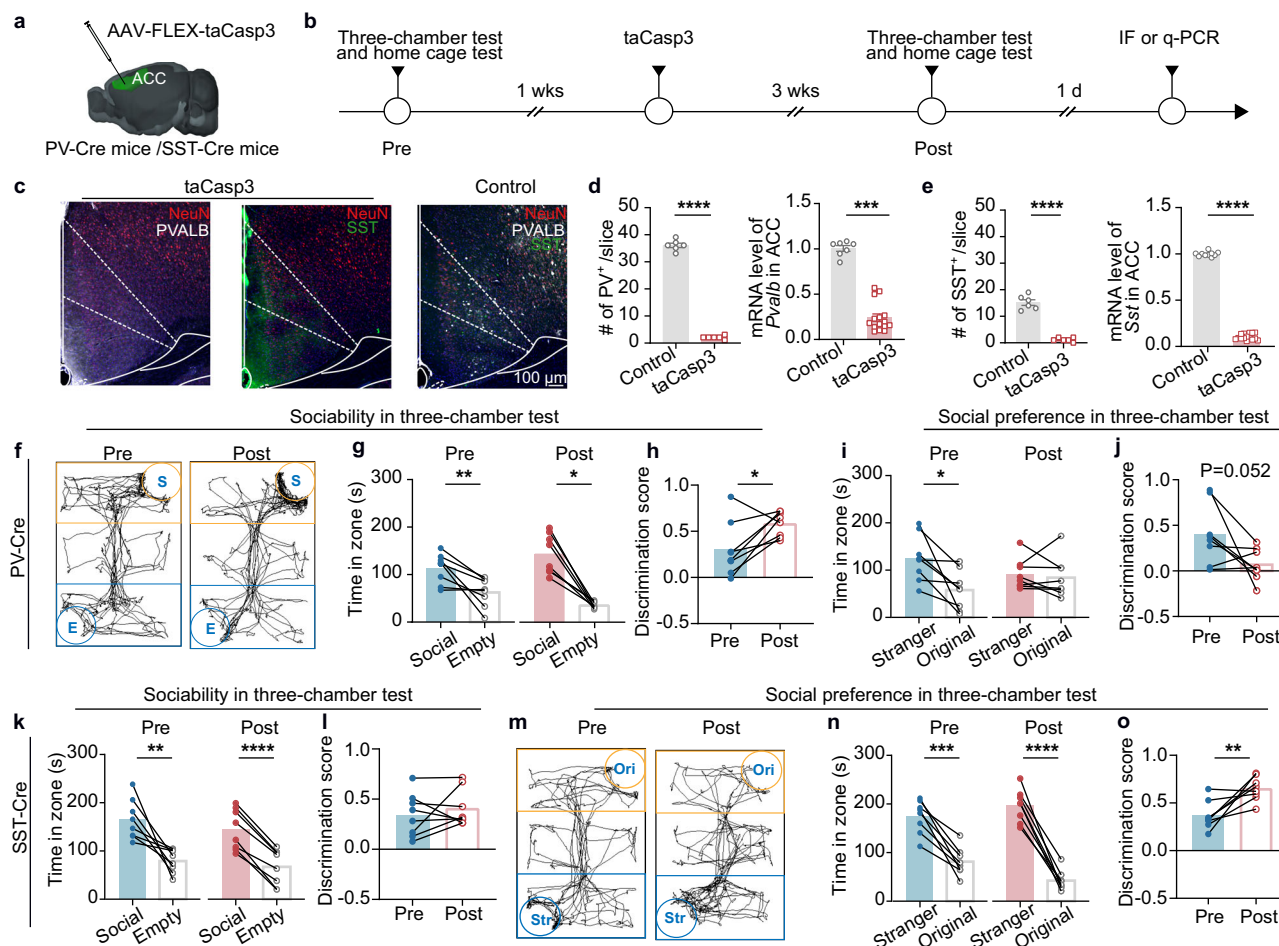


Fig. 2 | Apoptosis of PV and SST interneurons in the ACC induced by virus alters behavior in the three-chamber test. **a** Schematic diagram of virus injection (The 3D brain image was created with CEBIT/ION Digital Brain <https://www.digital-brain.cn/>). **b** Timeline of the experimental procedure. **c** Representative immunofluorescence images. **d** Number of PV⁺ cells (left) and *Pvalb* mRNA levels (right) (left: $n = 6$ slices from 2 mice per group, two-tailed unpaired t test, $t = 39.703$, $P < 0.0001$; right: $n = 7$ control mice, $n = 15$ taCasp3 mice, Two-sided Mann–Whitney U test, $Z = -3.702$, $P = 0.0002$). **e** Same as (**d**) but for SST-Cre mice (left: $n = 6$ slices from 2 mice per group, two-tailed unpaired separate variance estimation t test, $t = 12.494$, $P < 0.0001$; right: $n = 10$ mice for the control and $n = 15$ mice for taCasp3, two-tailed unpaired t test, $t = 73.364$, $P < 0.0001$). **f** Traces of PV-Cre mice before (left) and after (right) viral intervention in the sociability test. **g** Quantification of time spent in the social zone and empty zone before and after viral intervention for PV-Cre mice ($n = 8$ mice per group; two-tailed paired t test, $t = 3.519$, $P = 0.0097$ for Pre; Two-sided Wilcoxon signed-rank test, $Z = -2.521$, $P = 0.012$ for Post). **h** Discrimination score for PV-Cre mice in (**g**) ($n = 8$ mice, two-tailed paired t test, $t = -2.698$, $P = 0.031$). **i** Quantification of time spent in the stranger zone and original zone before and after viral intervention for PV-Cre mice ($n = 8$ mice, two-tailed paired t test, $t = 3.220$, $P = 0.015$ for Pre, $t = 0.620$, $P = 0.555$ for Post). **j** Discrimination score for PV-Cre mice in (**i**) ($n = 8$ mice, two-tailed paired t test, $t = 2.337$, $P = 0.052$). **k** Same as (**g**) but for SST-Cre mice ($n = 8$ mice; two-tailed paired t test, $t = 4.024$, $P = 0.005$ for Pre; $t = 11.084$, $P < 0.0001$ for Post). **l** Same as (**h**) but for SST-Cre ($n = 8$ mice, Two-sided Wilcoxon signed-rank test, $Z = -0.560$, $P = 0.575$). **m** Traces of SST-Cre mice before (left) and after (right) viral intervention in the social preference test. **n** Same as (**i**) but for SST-Cre mice ($n = 8$ mice; two-tailed paired t test, $t = 6.899$, $P = 0.0002$ for Pre; $t = 11.919$, $P < 0.0001$ for Post). **o** Same as (**j**) but for SST-Cre mice ($n = 8$ mice, two-tailed paired t test, $t = -3.615$, $P = 0.0086$). All statistical tests are two-sided. Data are presented as mean \pm SEM. * $P < 0.05$, ** $P < 0.01$, *** $P < 0.001$, **** $P < 0.0001$. Source data are provided as a Source Data File.

activation of PV interneurons shifted their preference toward the empty zone (ON, Fig. 4a, b middle), with no recovery to baseline after laser cessation (OFF2, Fig. 4a, b right; and Supplementary Movie 1). The social discrimination score significantly decreased between OFF1 and ON phases, as well as OFF1 and OFF2 phases (Supplementary Fig. 5a left). SST-Cre mice also exhibited a preference for the social zone before the laser stimulation (OFF1, Fig. 4g, h left). During laser stimulation, their sociability decreased (ON, Fig. 4g, h middle), but their preference for the social zone was restored after the stimulation ceased (OFF2, Fig. 4g, h right). Discrimination scores significantly decreased between OFF1 and ON phases but showed no difference between OFF1 and OFF2 phases (Supplementary Fig. 5b left). These results indicate that while both PV and SST interneuron activation reduces sociability, their effects exhibit distinct profiles.

In the social preference stage, PV-Cre mice displayed reduced preference for the stranger mouse during laser activation (ON, Fig. 4d, e middle), with no recovery post stimulation (OFF2, Fig. 4e right). The discrimination scores significantly decreased during the ON phase compared to OFF1 (Fig. 4f). In contrast, SST-Cre mice shifted preference from the stranger to the familiar mouse zone during laser activation (Fig. 4j, k left and middle). This altered preference persisted even after the laser was turned off (OFF2, Fig. 4j, k right; Supplementary Movie 2). SST-Cre mice exhibited negative discrimination scores during the ON phase, in contrast to PV-Cre mice (Fig. 4f, l). While discrimination scores remained stable between the OFF1 and OFF2 phases in PV-Cre mice, they continued to decline in SST-Cre mice (Supplementary Fig. 5a right, b right). Compared with the EYFP control group, both PV-Cre and SST-Cre mice expressing Chr2 exhibited reduced discrimination scores during

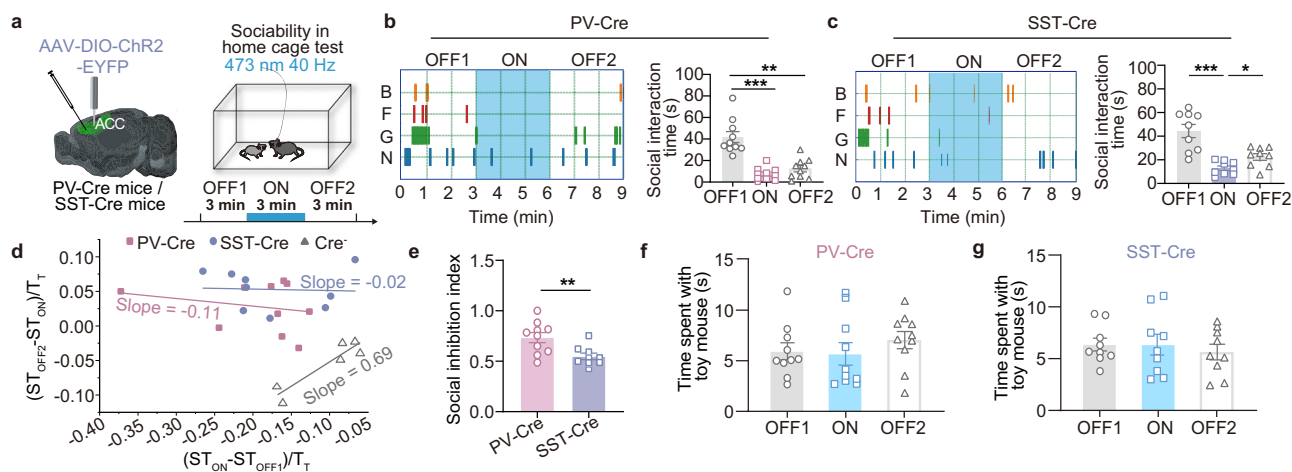


Fig. 3 | Optogenetic activation of PV or SST interneurons suppresses social behavior in the home cage test. **a** Schematic diagram of AAV-DIO-ChR2-EYFP injection into the ACC of PV-Cre mice and SST-Cre mice (left, the 3D brain image was created with CEBISIT/ION Digital Brain <https://www.digital-brain.cn/>) and diagram of the home cage test with laser delivery strategy (right panel is designed by us). **b** Optogenetic stimulation of PV interneurons modulates social behaviors in the home cage test. Left: The raster plot of different types of social behavior in the home cage test; B body contact, F following, G genital contact, N nose contact. Right: Statistical analysis of total social interaction time ($n = 10$ mice, Friedman's M test, $\chi^2 = 15.800$, $P = 0.0004$). **c** Same as (**b**) but for SST-Cre mice ($n = 9$ mice, Friedman's M test, $\chi^2 = 16.222$, $P < 0.0001$). **d** Comparison of slope coefficient in the PV-Cre, SST-Cre and Cre negative groups: X-axis: ST_{ON} (social time when laser ON)

$-ST_{OFF1}$ (social time during OFF1)/ T_T (total time of test); Y-axis: ST_{OFF2} (social time during OFF2) $- ST_{ON}$ (social time when laser ON)/ T_T (total time of test) ($n = 10$ mice, Spearman correlation test, $r = -0.055$, $P = 0.881$ for PV; $n = 9$ mice, Pearson correlation test, $r = -0.133$, $P = 0.732$ for SST; $n = 6$ mice, Pearson correlation test, $r = 0.922$, $P = 0.009$ for Cre negative). **e** Comparison of the social inhibition index between the PV-Cre and SST-Cre groups ($n = 10$ PV-Cre mice, $n = 9$ SST-Cre mice, two-tailed unpaired t test, $t = 3.046$, $P = 0.007$). **f** Summary data of the time spent with toys for PV-Cre group in the OFF1, ON and OFF2 stages in the home cage ($n = 10$ mice, Friedman's M test, $\chi^2 = 0.800$, $P = 0.670$). **g** Same as (**f**) but for SST-Cre group ($n = 9$ mice, repeated-measures ANOVA, $F_{between\ group} = 0.375$, $P = 0.693$). All statistical tests are two-sided. Data are presented as mean \pm SEM. * $P < 0.05$, ** $P < 0.01$, *** $P < 0.001$. Source data are provided as a Source Data File.

laser activation (Supplementary Fig. 6a middle, c middle). PV-Cre mice maintained lower scores than controls even after the stimulation ceased, whereas SST-Cre mice returned to baseline during the OFF2 phase (Supplementary Fig. 6a right, c right). SST-Cre mice displayed persistent alterations in social preference during and after stimulation, whereas PV-Cre mice primarily exhibited sociability deficits (Supplementary Fig. 6b, d). These findings suggest that PV interneurons primarily regulate sociability, whereas SST interneurons have a more prominent influence on social preference in the three-chamber test.

During the sociability stage, the PV-Cre group showed a decreasing trend relative to the SST-Cre group within the laser ON phase (Supplementary Fig. 7a middle). SST-Cre mice exhibited delayed termination of their first social encounter with a novel object compared to PV-Cre mice during photostimulation in this stage (Fig. 4m and Supplementary Movies 3 and 4). Although photostimulation reduced sociability in both groups compared with the laser OFF1 condition, the decline in discrimination score between the ON and OFF1 phases was more pronounced in PV-Cre mice (Fig. 4n). In the social preference stage, PV-Cre mice showed a preference for the center zone during the ON phase, whereas SST-Cre mice showed no clear preference (Fig. 4p, q). During photostimulation, PV-Cre mice took longer to terminate their first social interaction with a stranger object compared to SST-Cre mice (Fig. 4o and Supplementary Movies 5 and 6). SST-Cre mice showed greater decline in discrimination scores during laser activation (Supplementary Fig. 7b middle). Moreover, SST interneuron activation caused a larger disparity in normalized discrimination scores, which inversely correlated with sociability outcomes, compared to PV interneuron activation (Fig. 4n, r). Importantly, locomotion was not affected by optogenetic stimulation (Supplementary Fig. 5c, d). Both PV and SST interneuron activation suppressed Fos expression induced by social interaction (Supplementary Fig. 8a–h), with PV interneurons exerting a stronger inhibitory effect on ACC pyramidal neuron excitability (Supplementary Fig. 8i–m). Together, these results indicated that while both PV and

SST interneurons contribute to sociability, SST interneurons play a more prominent role in regulating social preference.

Abnormal *Kcnh7* expression in PV and SST interneurons contributes to social deficits in an autistic mouse model

To investigate factors underlying atypical interneuron activity in ASD-related social deficits, we focused on *Shank3*, a high-risk autism gene linked to social impairments in mutant mice^{8,27–33}. Using single-cell RNA sequencing (scRNA-seq) of ACC tissues from wild-type (WT) and *Shank3* KO mice, we identified 17,661 high-quality cells, including 9391 WT cells and 8270 *Shank3* KO cells. Cell clustering was performed by Seurat³⁴, with cell type annotation based on singleR³⁵ and manual verification. We identified eight distinct cell-type clusters (Fig. 5a, b), with the representative marker genes *Pvalb* and *Sst* highlighted (Fig. 5c). Among the differentially expressed genes, *Kcnh7*, encoding the Kv11.3 potassium channel and associating with ASD²², was significantly downregulated in both PV and SST interneurons in *Shank3* KO mice (Fig. 5d, e). Single-cell qRT-PCR confirmed *Kcnh7* as the predominant Kv11 family gene expressed in these interneurons, with reduced expression in *Shank3* KO mice (Fig. 6a, b, f, g and Supplementary Fig. 9a–f). Functionally, *Shank3* KO mice exhibited increased excitability in PV and SST interneurons (Fig. 6c, d, h and i), along with the reduced ERG channel currents (Fig. 6e, j). Administration of E-4031, an Kv11 channel blocker, mimicked this hyperexcitability in WT mice (Supplementary Fig. 9g–j), suggesting that *Kcnh7* downregulation contributes to interneuron dysfunction in *Shank3* KO mice.

To directly test this, we used a Cre-dependent CRISPR-Cas9 approach to knockout *Kcnh7* in ACC PV and SST interneurons (Fig. 7a). Immunofluorescence confirmed successful viral targeting (Fig. 7b, c, i, j) and reduced KCNH7 levels (Fig. 7d, k). *Kcnh7* KO increased interneuron excitability, altering the half-width and the fast afterhyperpolarization (fAHP, Fig. 7e–g and l–n) and firing frequency (Fig. 7h, o). Behaviorally, *Kcnh7* KO in PV interneurons reduced sociability without affecting social preference (Fig. 8a–d),

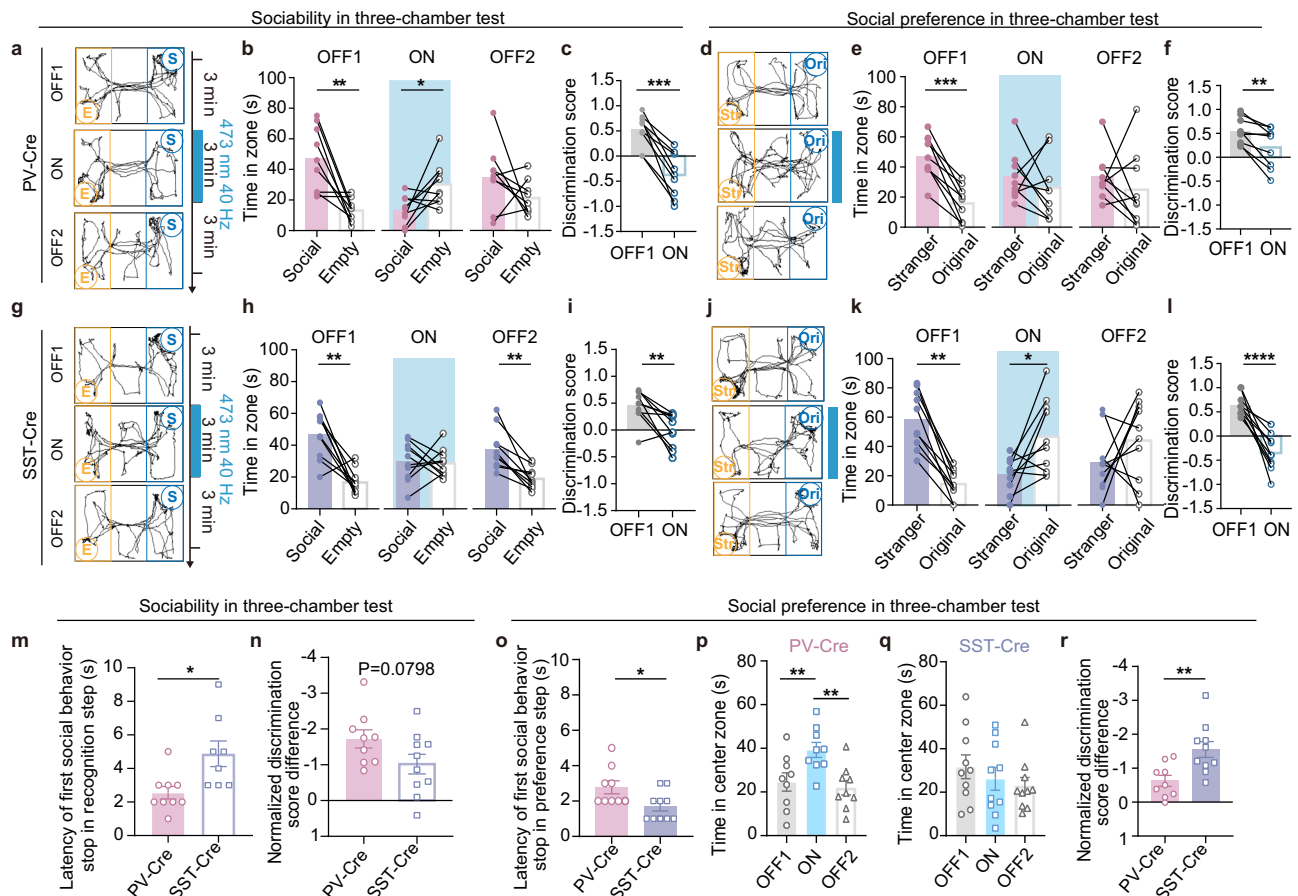


Fig. 4 | Optogenetic activation of PV or SST interneurons suppresses social interactions in the three-chamber. **a** Traces of PV-Cre mice in the sociability test. **b, c** Social interaction time (**b**) and discrimination score (**c**) from the sociability test ($n = 9$ mice, Wilcoxon signed-rank test, $Z = -2.666$, $P = 0.008$ for OFF1; two-tailed paired t test, $t = -2.516$, $P = 0.036$ for ON; two-tailed paired t test, $t = 1.544$, $P = 0.161$ for OFF2; two-tailed paired t test, $t = 6.805$, $P = 0.0001$ for discrimination score). **d** Traces of PV-Cre mice in the social preference test. **e, f** Same as (**b, c**) but in the social preference test ($n = 9$ mice, two-tailed paired t test, $t = 6.831$, $P = 0.0001$ for OFF1; $t = 0.827$, $P = 0.432$ for ON; $t = 0.830$, $P = 0.431$ for OFF2; $t = 3.833$, $P = 0.005$ for discrimination score). **g** Same as (**a**) but for SST-Cre mice. **h, i** Same as (**b, c**) but for SST-Cre mice ($n = 10$ mice, two-tailed paired t test, $t = 4.804$, $P = 0.001$ for OFF1; $t = 0.236$, $P = 0.819$ for ON; $t = 4.666$, $P = 0.001$ for OFF2; $t = 3.686$, $P = 0.005$ for discrimination score). **j** Same as (**d**) but for SST-Cre mice. **k, l** Same as (**e, f**) but for SST-Cre mice ($n = 10$ mice, Wilcoxon signed-rank test, $Z = -2.803$, $P = 0.005$ for

OFF1, $Z = -2.191$, $P = 0.028$ for ON; two-tailed paired t test, $t = -1.110$, $P = 0.296$ for OFF2, $t = 6.661$, $P < 0.0001$ for discrimination score). **m** Delay time when the first social behavior stopped during the sociability test ($n = 9$ PV-Cre mice, $n = 8$ SST-Cre mice; two-tailed unpaired t test, $t = -2.816$, $P = 0.013$). **n** Comparison of normalized discrimination scores in the sociability test ($n = 9$ PV-Cre mice, $n = 10$ SST-Cre mice, two-tailed unpaired t test, $t = -1.863$, $P = 0.079$). **o** Delay time when the first social behavior stopped in the stranger zone ($n = 9$ PV-Cre mice, $n = 10$ SST-Cre mice, Mann-Whitney U test, $Z = -2.195$, $P = 0.028$). **p, q** Time spent in the center zone for PV-Cre (**p**) and SST-Cre (**q**) in the social preference test ($n = 9$ mice, repeated-measures ANOVA, $P = 0.001$ for PV; $n = 10$ mice, Friedman's M test, $\chi^2 = 3.800$, $P = 0.150$ for SST). **r** Same as (**n**) but in the social preference test ($n = 9$ PV-Cre mice, $n = 10$ SST-Cre mice; two-tailed unpaired t test, $t = -3.164$, $P = 0.006$). All statistical tests are two-sided. Data are presented as mean \pm SEM. * $P < 0.05$, ** $P < 0.01$, *** $P < 0.001$, **** $P < 0.0001$. Source data are provided as a Source Data File.

while *Kcnh7* KO in SST interneurons impaired both sociability and social preference (Fig. 8e–h). SST-Cre mice exhibited a more pronounced social preference deficit compared to PV-Cre mice (Supplementary Fig. 10a–f). These results suggest that PV and SST interneurons play subtly yet demonstrably different roles in disorders involving social deficits and highlight the importance of *Kcnh7* in regulating interneuron function in the ACC, thereby influencing social behavior.

Specific projections contribute to the differential suppression of social behavior regulated by PV and SST interneuron activity in the ACC

Our results demonstrate that PV and SST interneurons differentially regulate social behavior, potentially due to distinct synaptic inputs and firing patterns (Supplementary Fig. 11). To investigate the neural circuits underlying these differences, we traced inputs to PV and SST interneurons in the ACC by injecting a mixture of AAV-EF1a-DIO-His-

EGFP-T2A-TVA and AAV-EF1a-DIO-oRVG into the ACC of the PV-Cre and SST-Cre mice. Three weeks later, a rabies virus (RV) was injected at the same site (Fig. 9a)³⁶. Both interneuron types received input from similar upstream afferents; however, PV interneurons were preferentially innervated by the lateral posterior thalamic nucleus (LPMR), whereas SST interneurons received stronger input from the ventral hippocampus (vHPC) (Fig. 9b–f and Supplementary Fig. 12a, b). Optogenetic stimulation and whole-cell patch-clamping recordings confirmed excitatory monosynaptic projections from the LPMR to PV interneurons and from the vHPC to SST interneurons in the ACC (Supplementary Fig. 13a–c). In vivo calcium imaging further validated the functional connectivity of these pathways (Supplementary Fig. 13d–i).

To assess the functional roles of these pathways, we selectively expressed ChR2 in PV or SST interneurons receiving input from the LPMR or vHPC (Fig. 10a–c, j–l). Approximately 50% of the PV and SST interneurons expressed ChR2, and over 90% of the ChR2-positive cells

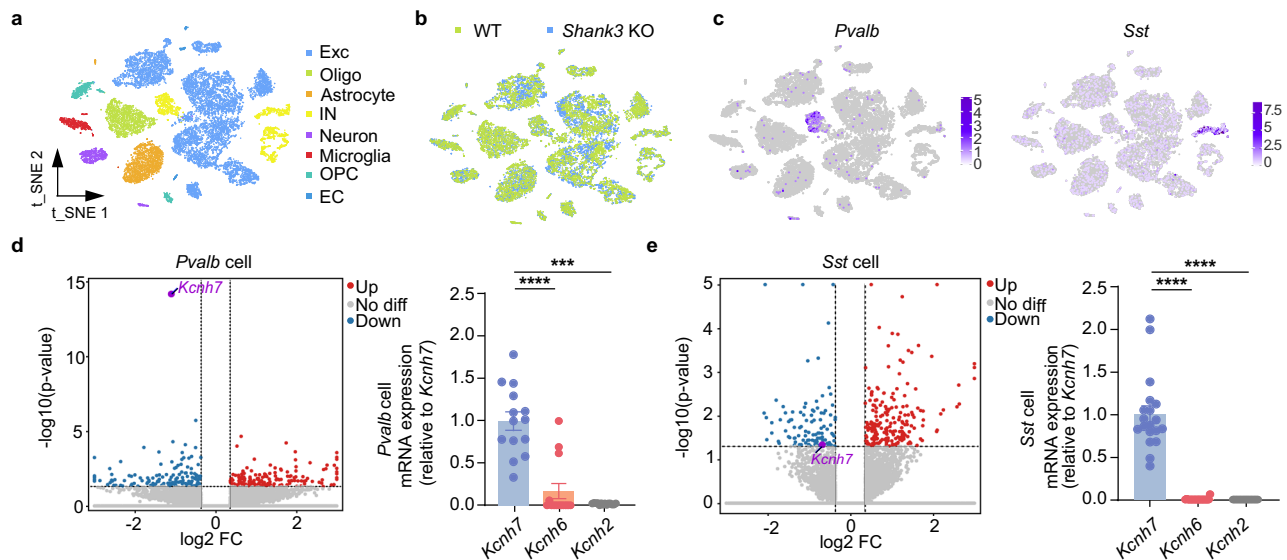


Fig. 5 | Decreased levels of *Kcnh7* in PV and SST interneurons within the ACC of *Shank3* KO mice. **a**, **b** t-SNE plots of WT and *Shank3* KO groups showing cell clusters, including oligodendrocyte (Oligo), oligodendrocyte precursor cell (OPC), endothelial cell (EC), interneuron (IN), and excitatory neuron (Exc). **c** Feature plots showing single-cell gene expression of known inhibitory neuron markers (*Pvalb*, left; *Sst*, right). **d** Volcano plot showing that *Kcnh7* is one of the downregulated differentially expressed genes in *Shank3* KO mice compared to the WT mice in PV

interneurons, identified by scRNA-seq (left). Relative mRNA expression showing that *Kcnh7* is more prominently in *Pvalb*-positive neurons compared to *Kcnh6* and *Kcnh2* (right, $n = 14$ cells from 2 mice; Kruskal–Wallis H test, $\chi^2 = 24.783$, $P < 0.0001$). **e** Same as **(d)** but for *Sst* neurons ($n = 19$ cells from 2 mice; Kruskal–Wallis H test, $\chi^2 = 41.128$, $P < 0.0001$). All statistical tests are two-sided. Data are presented as mean \pm SEM. *** $P < 0.001$, **** $P < 0.0001$. Source data are provided as a Source Data File.

in these two groups were either PV or SST interneurons (Supplementary Fig. 14a–d). Activation of the LPMR-PV(ACC) pathway significantly reduced sociability and social preference (Fig. 10d–i and Supplementary Fig. 15a, b), whereas the vHPC-PV(ACC) pathway had no effect (Supplementary Fig. 16a–d). In contrast, activation of the vHPC-SST(ACC) pathway impaired social preference without affecting sociability (Fig. 10m–q and Supplementary Fig. 15c, d), while the LPMR-SST(ACC) pathway had no impact (Supplementary Fig. 16e–h). Among other inputs, the mediodorsal thalamus (MD)-PV(ACC) pathway modestly reduced sociability (Supplementary Fig. 17a, b), while the MD-SST(ACC) pathway slightly impaired social preference (Supplementary Fig. 18c, d). Projections from the posterior thalamic nuclear group (Po) to PV(ACC) and from the claustrum/dorsal endopiriform nucleus (Cl/Den) to SST(ACC) had no effect on social interest in either the sociability or social preference tests (Supplementary Figs. 17c, d and 18a, b). The LPMR-PV(ACC) projection exerted the strongest influence on sociability, and the vHPC-SST(ACC) projection had the most pronounced effect on social preference (Supplementary Figs. 17e–h and 18e–i). Overall, these results highlight a greater impact of the LPMR-PV(ACC) projection on sociability, although it is not the sole regulator. In contrast, the vHPC-SST(ACC) projection has the strongest effect on social preference among the pathways studied.

Discussion

Projection neurons serve as functional executors within the brain, influencing neural functions through their intrinsic properties and the modulation of local interneurons via various regulatory mechanisms^{37,38}. This study focused on two primary interneuron subtypes, PV and SST interneurons, in the ACC. We found that both types of interneurons significantly influence social behavior through distinct and nuanced mechanisms. In a *Shank3* autism model, we observed a reduced expression of the *Kcnh7* gene, a known risk factor for ASD, specifically in PV and SST interneurons within the ACC. Deletion of *Kcnh7* in either PV or SST interneurons contributed to altered social interactions, highlighting the involvement of these interneuron subtypes in ASD-related behavioral variability. Furthermore, our pathway-

specific analyses revealed that the LPMR-PV(ACC) and vHPC-SST(ACC) projections underline the roles of PV and SST interneurons in regulating social behavior. The LPMR-PV(ACC) pathway exerted a stronger influence on sociability, whereas the vHPC-SST(ACC) pathway predominantly affected social preference. Overall, our findings demonstrate that PV and SST interneurons in the ACC play a critical role in regulating social interactions through distinct synaptic inputs and downstream circuit mechanisms.

Social interaction is commonly evaluated using tests like the three-chamber paradigm, which assesses sociability (stranger vs. empty chamber) and social preference (familiar vs. novel mouse). This setup allows the subject to explore and recognize the stranger mouse, providing a measure of its sociability. Social preference is evaluated in the second stage by introducing a familiar mouse in one chamber and a novel mouse in the other. This phase evaluates the subject's tendency to interact with a familiar versus a new conspecific^{8,39}. By analyzing the time spent in each chamber, researchers can quantify social interest while minimizing variability caused by the mouse's internal state. By integrating social tests with various interventions, we found that PV and SST interneurons are involved in social interaction within subtly different ways. PV interneuron ablation increased sociability, while their activation through three different methods reduced it, indicating a pronounced role in regulating sociability. However, their influence on social preference varies across methodologies, likely due to differences in experimental approaches. Apoptosis induced permanent PV interneuron ablation²⁵, likely resulting in a minimal number of surviving cells capable of generating a compensatory effect. In contrast, somatic and pathway-specific optogenetics produced acute, reversible effects, with the latter being less robust. Furthermore, *Kcnh7* knockout moderately enhanced neuronal excitability. Thus, if social preference is less sensitive to PV neuron regulation, the outcomes across different manipulations may vary accordingly (Supplementary Fig. 19). Similarly, the four strategies used to manipulate SST interneurons produced consistent effect on social preference, while their impact on sociability was more variable. These results suggest that SST neurons may be more actively involved in social preference. This

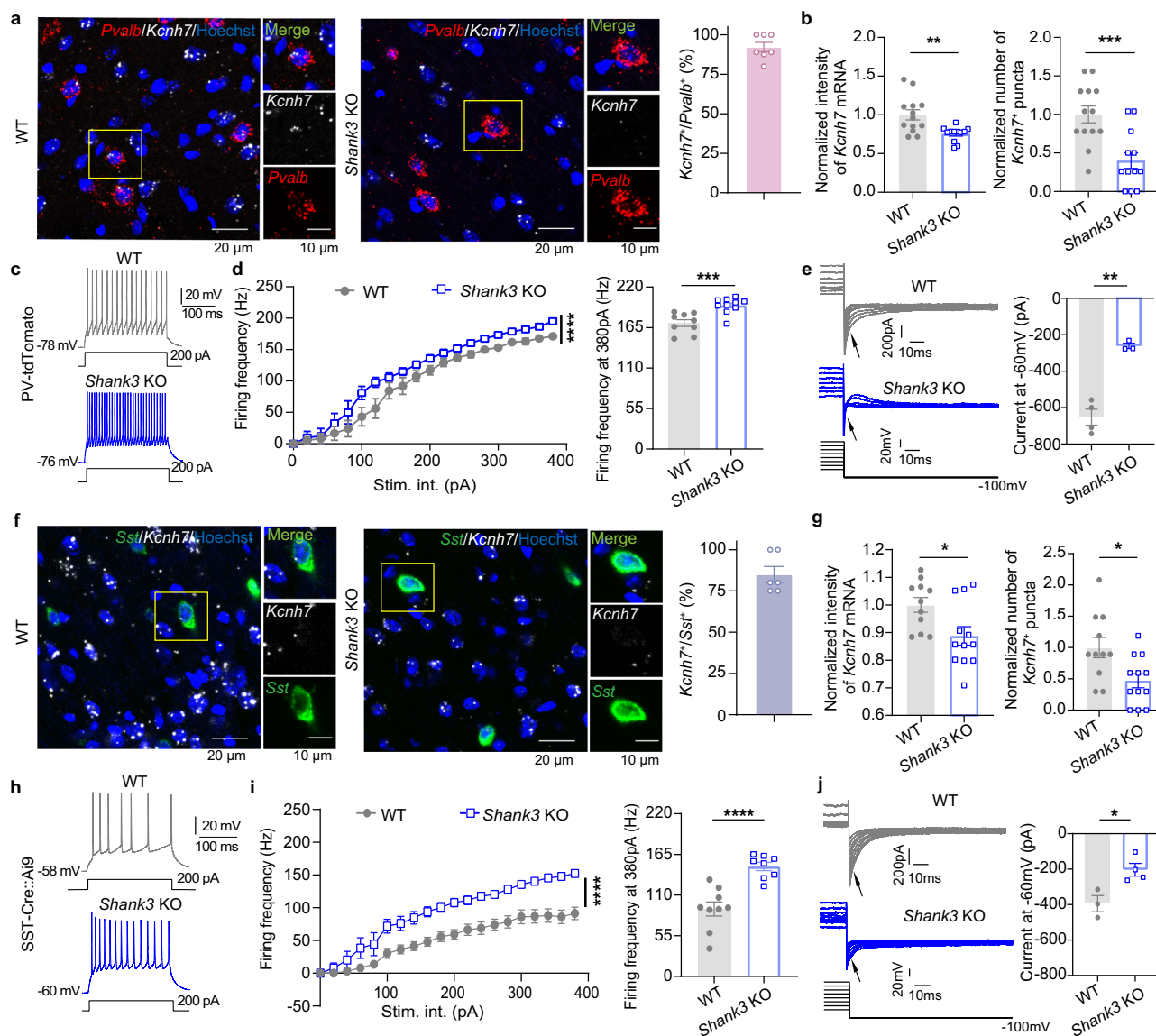


Fig. 6 | Increased excitability and decreased Kv11.3 current in PV and SST interneurons within the ACC of *Shank3* KO mice. **a** RNAscope showing *Kcnh7* (gray) and *Pvalb* (red) expression in WT (left) and *Shank3* KO mice (middle), with the quantification of *Kcnh7*/*Pvalb*⁺ ratio (right, $n = 7$ slices from 2 mice). **b** Normalized fluorescence intensity of *Kcnh7* (left) and normalized number of *Kcnh7*⁺ puncta (right) in *Pvalb*⁺ neurons ($n = 13$ cells in WT and $n = 12$ cells in KO from 3 mice per group; Mann–Whitney U test, $Z = -2.940$, $P = 0.003$ for intensity; two-tailed unpaired t test, $t = 3.811$; $P = 0.0009$ for puncta number). **c** Action potential trace at 200 pA in PV-tdTomato mice. **d** Input–output curve (left) and spike frequency at 380 pA (right) (Stim. int.: stimulus intensity; $n = 9$ cells in WT and $n = 10$ cells in KO from 3 mice per group, Friedman’s M test, $\chi^2_{\text{between group}} = 27.676$, $P_{\text{between group}} < 0.0001$, $\chi^2_{\text{within group}} = 354.809$, $P_{\text{within group}} < 0.0001$ for input–output; two-tailed unpaired t test, $t = -4.274$, $P = 0.0005$ for frequency at 380 pA). **e** Representative traces of the Kv11.3 current (left) and quantification (right) ($n = 4$

cells for the WT and $n = 3$ cells for the KO group from 2 mice per group; two-tailed unpaired t test, $t = -8.416$, $P = 0.002$). **f** Same as (a) but for *Sst*⁺ interneurons (right, $n = 6$ slices from 2 mice). **g** Same as (b) but for *Sst*⁺ interneurons ($n = 11$ cells for the WT and $n = 12$ cells for the KO from 3 mice per group, two-tailed unpaired t test, $t = 2.583$, $P = 0.017$ for intensity, $t = 2.724$, $P = 0.013$ for puncta number). **h** Same as (c) but for SST-Cre::Ai9 neurons. **i** Same as (d) but for SST-Cre::Ai9 neurons ($n = 9$ cells in WT and $n = 8$ cells in KO from 3 mice per group, Friedman’s M test, $\chi^2_{\text{between group}} = 76.699$, $P_{\text{between group}} < 0.0001$, $\chi^2_{\text{within group}} = 297.776$, $P_{\text{within group}} < 0.0001$ for input–output; two-tailed unpaired t test, $t = -5.013$, $P < 0.0001$ for frequency at 380 pA). **j** Same as (e) but for SST-Cre::Ai9 neurons ($n = 3$ cells in WT and $n = 4$ cells in KO from 2 mice per group, two-tailed unpaired t test, $t = -3.350$, $P = 0.020$). All statistical tests are two-sided. Data are presented as mean \pm SEM. * $P < 0.05$, ** $P < 0.01$, *** $P < 0.001$, **** $P < 0.0001$. Source data are provided as a Source Data File.

conclusion is further supported by comparing the effects of PV and SST interneuron modulation.

Although activating either PV or SST interneurons significantly reduced sociability compared to the EYFP control group, a notable distinction was evident during the OFF2 phase. During the social preference phase, SST interneuron activation strongly inhibited behavior, whereas PV interneurons activation had no effect. Nevertheless, we cannot entirely exclude the potential influence of SST interneurons on sociability or the involvement of PV interneurons in social preference.

Investigating the underlying mechanisms could provide further insights into the distinct roles of these interneuron subtypes in regulating social behavior. Additionally, we observed reduced PV and SST interneuron activity when mice approached an empty area, suggesting the empty cage may act as a novel object. Since the ACC regulates responses to novelty related information⁴⁰, these interneurons likely process object-related information. Furthermore, neuronal activity during social interactions differed between the home cage and the three-chamber tests. The home cage setting introduces only an

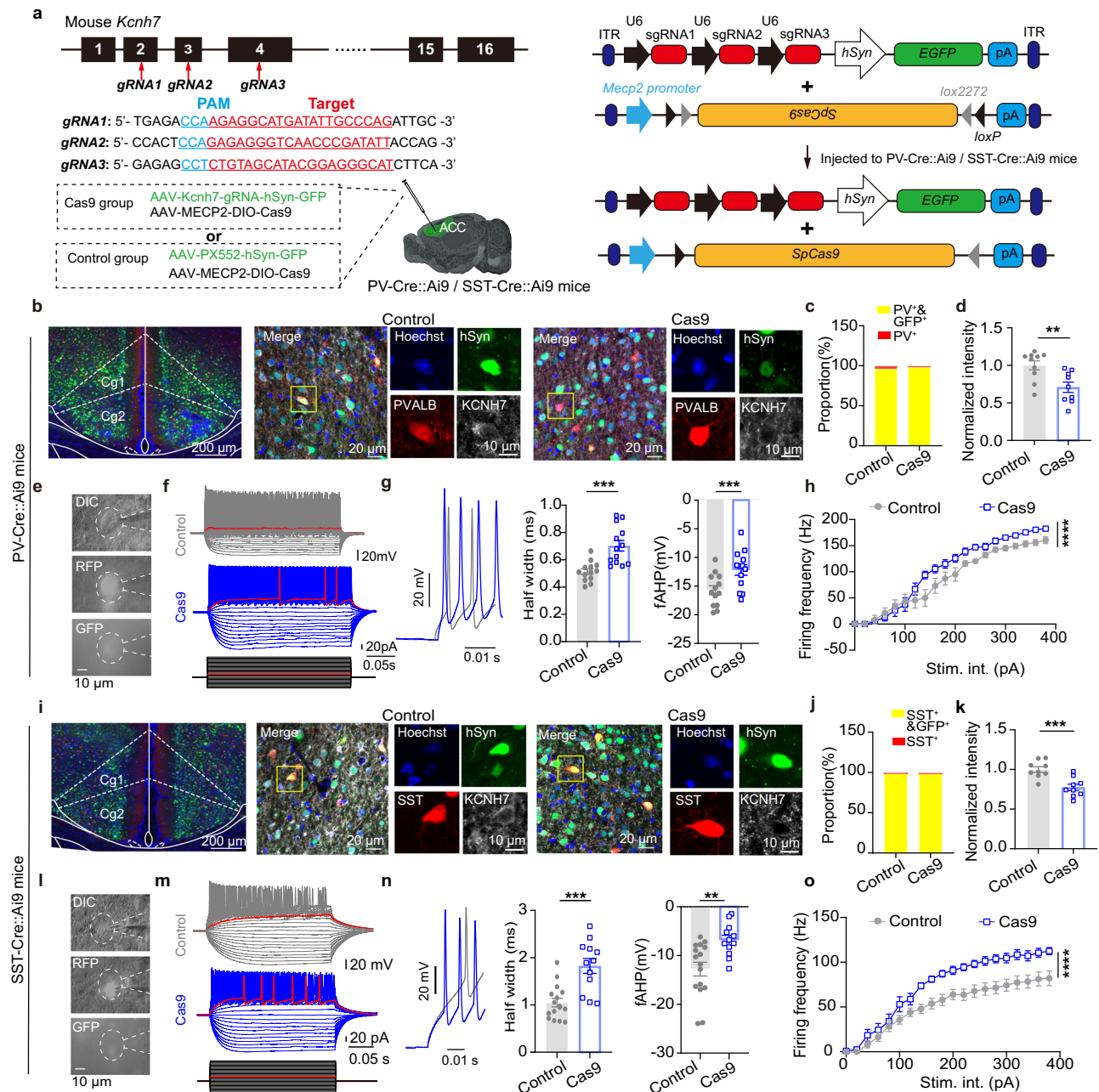


Fig. 7 | CRISPR-Cas9-mediated *Kcnh7* knock out in PV and SST interneurons enhances neuronal excitability. **a** Schematic of the CRISPR-Cas9 viral strategy used to target *Kcnh7* in PV and SST interneurons (The 3D brain image was created with CEBST/ION Digital Brain <https://www.digital-brain.cn/>). **b** Representative images of PV-Cre mice showing AAV-sgRNA-hSyn-GFP expression (left) and KCNH7 expression in the control group (middle) and Cas9 virus group (right). **c** Over 99% of PV⁺ neurons expressed GFP, indicating successful viral infection ($n = 6$ slices for 2 mice per group). **d** Quantification of KCNH7 protein levels showing a significant reduction in the Cas9 group compared to the control group ($n = 10$ cells for Control and $n = 9$ cells for Cas9 from 2 mice per group; Mann-Whitney U test, $Z = -2.776$; $P = 0.006$). **e** Ex vivo electrophysiological recordings from PV-Cre::Ai9 neuron. **f, g** Representative traces of action potential (**f**), half width (**g** left, middle) and fAHP (**g** right) in PV-Cre::Ai9 cells ($n = 13$ cells per group from 3 mice; two-tailed unpaired t test, $t = -4.342$, $P = 0.0004$ for half width; two-tailed unpaired t test, $t = -2.914$, $P = 0.008$ for fAHP). **h** Input-output curve of PV-Cre::Ai9 neurons, showing

increased spike frequency in the Cas9 group compared to the control group ($n = 9$ control cells and $n = 12$ Cas9 cells from 3 mice per group; Friedman's M test; $\chi^2_{\text{between group}} = 26.390$; $P_{\text{between group}} < 0.0001$; $\chi^2_{\text{within group}} = 346.474$; $P_{\text{within group}} < 0.0001$). **i** Same as (**b**) but for SST-Cre mice. **j** Over 99% of SST⁺ neurons expressed GFP indicating successful viral infection ($n = 6$ slices for 2 mice per group). **k** Significant reduction in KCNH7 protein levels in the Cas9 group compared to the control group ($n = 9$ cells from 2 mice per group, two-tailed unpaired t test, $t = 4.189$, $P = 0.0007$). **l–n** Same as (**e–g**) but for SST-Cre::Ai9 cells ($n = 16$ cells for control and $n = 12$ cells for Cas9 from 3 mice per group; two-tailed unpaired t test, $t = -4.568$, $P = 0.0001$ for half width; Mann-Whitney U test, $Z = -2.971$, $P = 0.003$ for fAHP). **o** Same as (**h**) but for SST-Cre::Ai9 cells ($n = 10$ cells for control and $n = 12$ cells for Cas9 from 3 mice per group; Friedman's M test, $\chi^2_{\text{between group}} = 111.364$; $P_{\text{between group}} < 0.0001$, $\chi^2_{\text{within group}} = 330.163$, $P_{\text{within group}} < 0.0001$). All statistical tests are two-sided. Data are presented as mean \pm SEM. ** $P < 0.01$, *** $P < 0.001$, **** $P < 0.0001$. Source data are provided as a Source Data File.

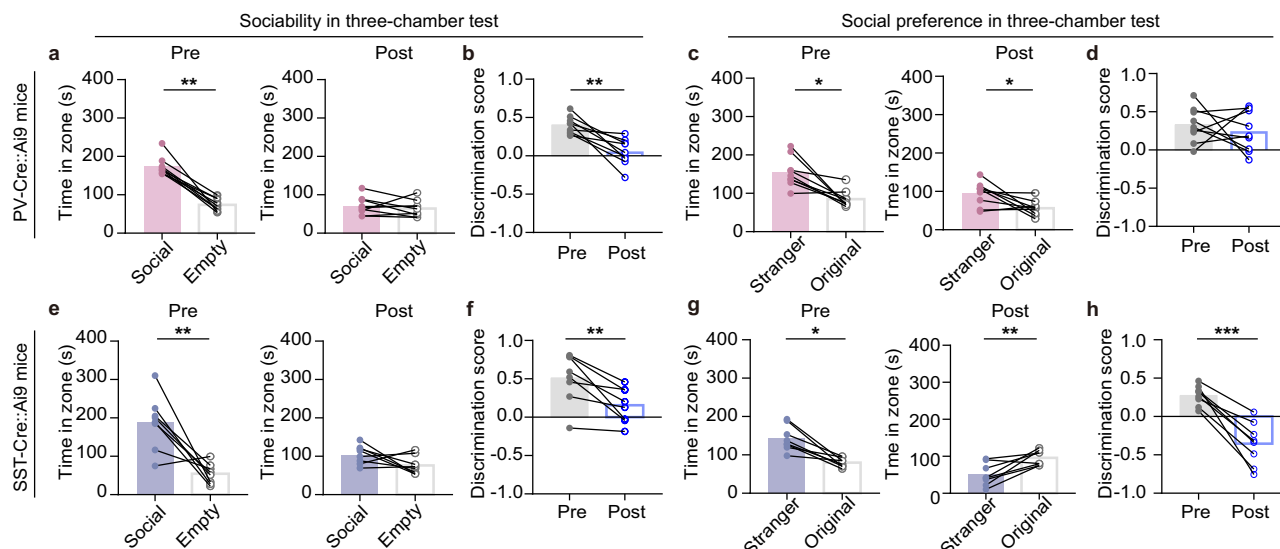


Fig. 8 | Knockout of *Kcnh7* by CRISPR-Cas9 in PV and SST interneurons impairs social interaction. **a** Time spent in the social zone and empty zone before and after viral intervention in PV-Cre mice during the sociability test ($n = 9$ mice, Wilcoxon signed-rank test, $Z = -2.666$, $P = 0.008$ for Pre; two-tailed paired t test, $t = 0.787$, $P = 0.454$ for Post). **b** Comparison of discrimination score for PV-Cre mice in the sociability test ($n = 9$ mice, two-tailed paired t test, $t = 4.775$, $P = 0.001$). **c** Time spent in the stranger zone and original zone before and after viral intervention in PV-Cre mice during the social preference test ($n = 9$ mice, Wilcoxon signed-rank test, $Z = -2.547$, $P = 0.011$ for Pre; two-tailed paired t test, $t = 2.858$, $P = 0.021$ for Post). **d** Comparison of discrimination score for PV-Cre mice in the social preference test ($n = 9$ mice, two-tailed paired t test, $t = 0.651$, $P = 0.533$). **e** Time spent in

the social zone and empty zone before and after viral intervention in SST-Cre mice during the sociability test ($n = 8$ mice, two-tailed paired t test, $t = 4.151$, $P = 0.004$ for Pre, $t = 1.855$, $P = 0.106$ for Post). **f** Comparison of discrimination score for SST-Cre mice in the sociability test ($n = 8$ mice, two-tailed paired t test, $t = 3.874$, $P = 0.006$). **g** Time spent in the stranger zone and original zone before and after viral intervention in SST-Cre mice during the social preference test ($n = 8$ mice, Wilcoxon signed-rank test, $Z = -2.521$, $P = 0.012$ for Pre; two-tailed paired t test, $t = -3.765$, $P = 0.007$ for Post). **h** Comparison of discrimination score for SST-Cre mice in the social preference test ($n = 8$ mice, two-tailed paired t test, $t = 7.011$, $P = 0.0002$). All statistical tests are two-sided. Data are presented as mean \pm SEM. * $P < 0.05$, ** $P < 0.01$, *** $P < 0.001$. Source data are provided as a Source Data File.

unfamiliar conspecific, whereas the three-chamber test involves both a novel environment and an unfamiliar mouse, potentially confounding the evaluation of social behavior⁴¹. This implies that the ACC processes diverse socially relevant information, with some overlap between social and object-related inputs⁴⁰. Notably, PV and SST interneurons showed reduced responses to both novel objects and conspecifics, but their suppression was stronger during interactions with novel mice.

Our findings reveal distinct roles of PV and SST interneurons in social interaction, driven by their unique connectivity and physiological properties. PV interneurons form synapses onto the cell bodies of nearby pyramidal neurons, eliciting stronger inhibitory postsynaptic currents (oIPSCs) and significantly suppressing the excitability of ACC pyramidal neurons in vivo. In contrast, SST interneurons primarily target the distal dendrites of pyramidal neurons, generating relatively smaller oIPSCs and modulating synaptic integration through a distinct spatial and functional mechanism³⁸. Both types inhibit Fos expression induced by social behavior, with PV interneurons exhibit stronger inhibition (Supplementary Fig. 8). Additionally, previous studies have shown that PV and SST interneurons display different long-term¹⁶ or short-term synaptic plasticity¹⁷ and fire at distinct theta cycle phases^{42,43}, enabling differential regulation of pyramidal neuron responses to excitatory inputs. These distinctions allow PV and SST interneurons to fine-tune ACC activity during social information processing, contributing to the precise regulation of social behavior.

Our findings suggest that PV and SST interneurons are crucial for regulating social interactions, partially shaped by their synaptic inputs. While PV and SST interneurons share some inputs, they also exhibit significant differences. LPMR projections to PV interneurons in the ACC regulate sociability for both social objects and novel social objects, whereas vHPC projections to SST interneurons in the ACC modulate social preference. The LPMR, part of the attention network⁴⁴,

connects with the visual cortex, parietal cortex, and ACC. Imaging studies demonstrate that the pulvinar region of the brain, which is equivalent to the LP (lateral posterior nucleus) region in mice, has structural abnormalities in individuals with autism^{45,46}. The vHPC is associated with social preference^{47,48}, while other regions such as the MD, play a lesser role (Supplementary Fig. 18). In the ACC, VIP interneurons represent another type of interneuron that inhibits PV and SST interneurons, thereby disinhibiting pyramidal cells upon activation¹⁸. A study on the disinhibitory effect of VIP interneuron in the microcircuit of the mPFC¹⁴ suggests that VIP interneurons may also influence the ACC and social behavior. While our study emphasizes specific projections to PV and SST interneurons, further research is needed to explore how upstream regions regulate other interneurons, such as VIP, and their impact on social behavior.

The number of upstream neurons could also influence the function of projection neurons. For example, LPMR projection neurons, which minimally target SST interneurons in the ACC, might not significantly affect social behavior through SST interneurons. Additionally, we cannot entirely exclude the potential influence of long-range GABAergic projections from other upstream regions on PV and SST interneuron activity during social processing^{49,50}. Moreover, the long-range projection to the upstream regions of PV and SST interneurons may also contribute to the modulation of social behavior⁵¹. Abnormal activation of PV or SST interneurons in the ACC could contribute to the aberrant social behavior, indicating that dysregulated upstream projections targeting these interneurons could be a critical factor contributing to such abnormalities. Thus, normal ACC activity during social recognition likely depends on the interaction between upstream projections and local circuits. Quantifying these contributions and developing mathematical models to describe the regulation of pyramidal neurons by PV and SST interneurons could elucidate their roles in social interaction and related behaviors.

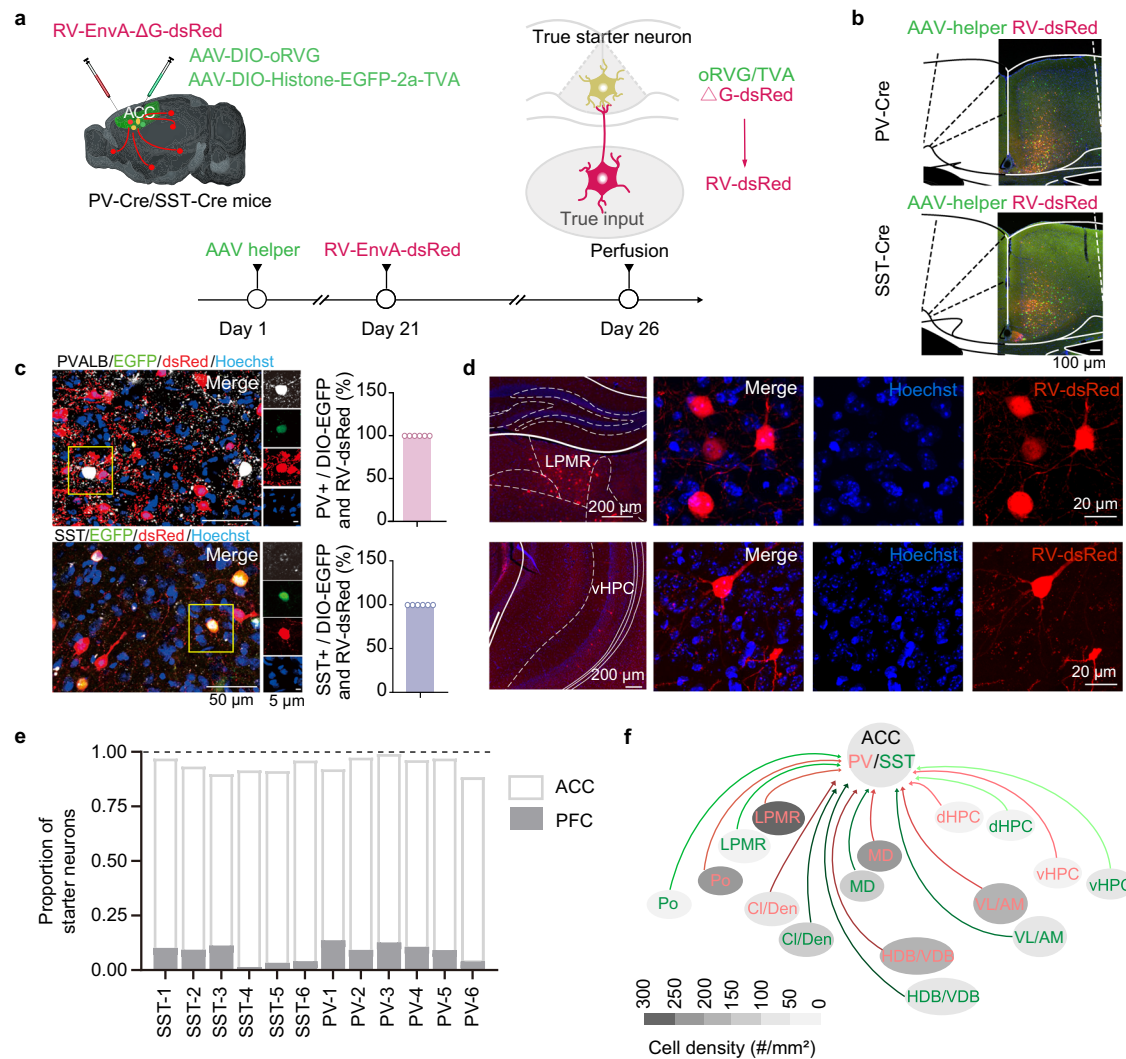


Fig. 9 | Retrograde monosynaptic tracing reveals that the LPMR and vHPC preferentially project to PV and SST interneurons in the ACC. **a** Schematic of experimental design (The 3D brain image was created with CEBISIT/ION Digital Brain <https://www.digital-brain.cn/> and the right panel is designed by us). **b** Representative images showing the starter neurons in ACC from a PV-Cre and a SST-Cre mice. **c** Representative images showing starter neurons in the ACC co-expressing AAV-helper (His-EGFP, oRVG), RV-dsRed, and PV or SST (gray) ($n = 6$ slices from 3 mice per group). **d** PV interneurons in the ACC receive direct inputs from the LPMR (top), while SST interneurons in the ACC receive direct inputs from the vHPC (bottom). Images are from representative animals of each group.

e Quantification of principal starter neurons (expressing His-EGFP and RV-dsRed) in the ACC and PFC ($n = 6$ mice per group). The value 1.00 indicates all detected starter neurons. **f** Analysis of RV-dsRed-positive cell density in upstream brain region ($n = 5$ mice per group). Po posterior thalamic nucleus, LPMR lateral posterior thalamic nucleus, mediodorsal part, Cl/Den claustrum/dorsal endopiriform nucleus, MD mediodorsal thalamus, HDB/VDB nucleus of the horizontal/vertical limb of the diagonal band, VL/AM ventrolateral thalamic nucleus/anteromedial thalamic nucleus, dHPC dorsal hippocampus, vHPC ventral hippocampus. Data are presented as mean \pm SEM. Source data are provided as a Source Data File.

Our study highlights the differential roles of PV and SST interneurons in social deficits associated with disorders like ASD. These interneuron subtypes exhibit distinct responses to stimuli in the hippocampus⁵² and cortex^{14,15}, with genetic manipulations, such as *Mecp2* KO in PV or SST interneurons producing varied phenotypes of Rett syndrome⁵³. We found that *Kcnh7*, an ASD susceptibility gene, selectively modulates the function of PV and SST interneurons, influencing social behavior across different interaction stages. In *Shank3* KO mice, a model of autism, *Kcnh7* downregulation increased interneuron excitability, correlating with impaired social interactions (Figs. 5, 6, and 8). Optogenetic experiments also revealed similar impairments in social interactions (Figs. 3 and 4). Our findings suggest that *Kcnh7* may be a key modulator of interneuron function and that phenotypic abnormalities in *Shank3* KO mice involve dysfunction in both pyramidal neuron and interneuron. Indeed, we found that sensory hypersensitivity in *Shank3* KO mice was linked to GABAergic

interneuron defects⁵⁴. These findings highlight the complex interplay between molecular factors (such as *Shank3* and *Kcnh7*), cellular processes involving PV and SST interneurons, projection neurons and behavioral outcomes. This deeper understanding of how these elements interact offers valuable insights into the neurobiological basis of social dysfunction and its related disorders.

To our knowledge, the present research provides strong evidence that PV and SST interneurons in the ACC play differential roles in social interaction. These nuanced roles likely contribute to the various manifestations of social interaction deficits. This insight not only enhances our understanding of social behavior but also opens new avenues for addressing related disorders, particularly autism. By targeting the specific functions of PV and SST interneurons within the ACC complex network, novel therapeutic approaches may be developed underlying the new mechanisms of social dysfunction.

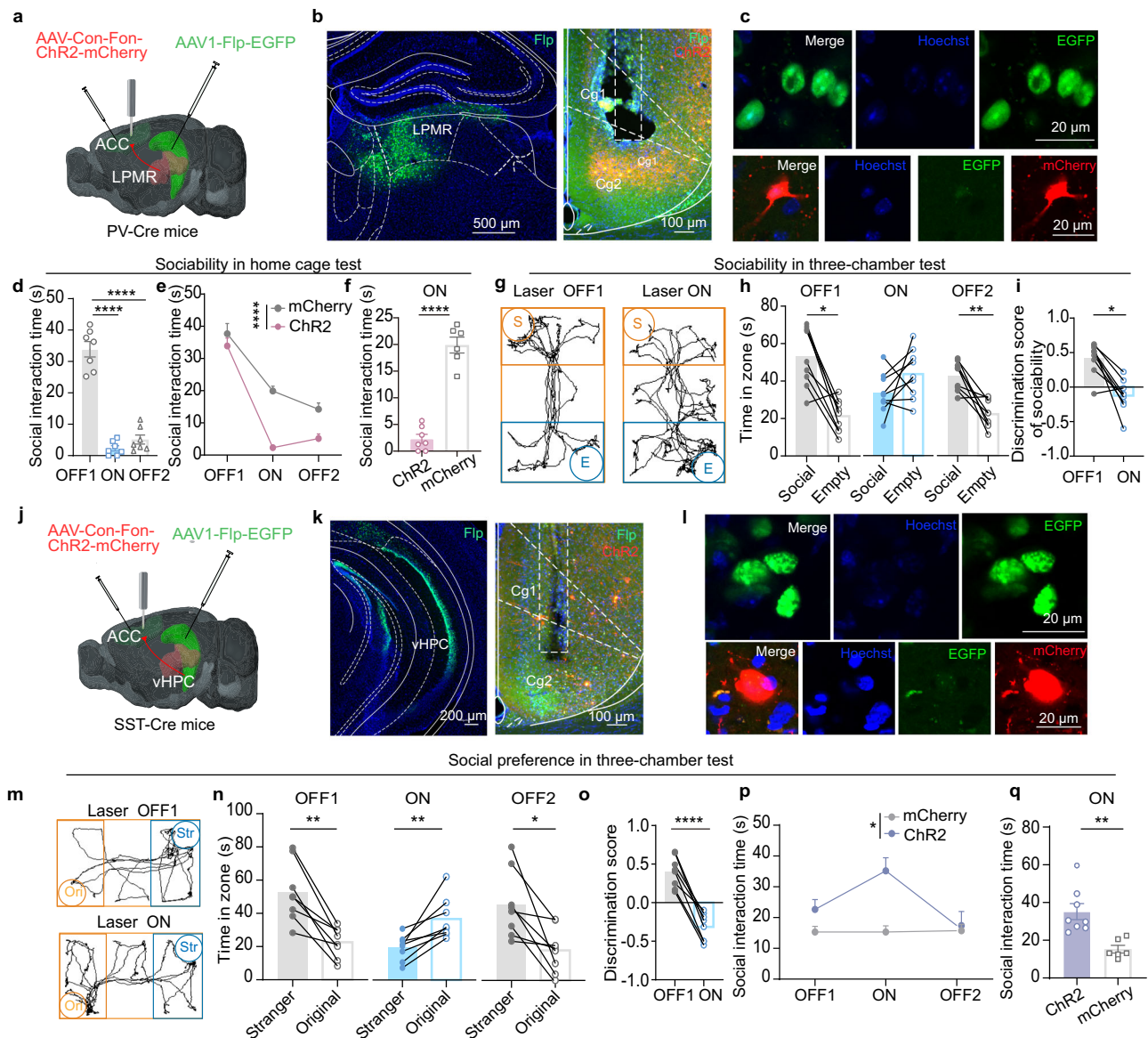


Fig. 10 | Selective activation of the LPMR-PV (ACC) or vHPC-SST (ACC) projection impairs social interaction. **a** Schematic diagram of virus strategy and optic fibers implantation site. **b** Injection site in LPMR (left) and ACC (right). **c** AAV1 expression in LPMR (top) and co-labeling of AAV1-EGFP and Chr2-mCherry in ACC of PV-Cre mice (bottom). **d** Social interaction time in the home cage test ($n = 7$ mice, repeated-measures ANOVA, $F_{\text{between group}} = 78.499$, $P < 0.0001$). **e**, **f** Social interaction time between the Chr2 and mCherry control groups in different laser stages (**e**: $n = 7$ mice for Chr2, $n = 6$ mice for mCherry; repeated-measures ANOVA, $F_{\text{between group}} = 36.693$, $P < 0.0001$, $F_{\text{within group}} = 111.555$, $P < 0.0001$) and quantification of social time when the laser ON (**f**: two-tailed unpaired t test, $t = -10.678$, $P < 0.0001$). **g** Representative movement traces of PV-Cre mice during the sociability test. **h**, **i** Social interaction time of PV-Cre mice during different laser stages (**h**: $n = 9$ mice, Wilcoxon signed-rank test, $Z = -2.547$, $P = 0.011$ for laser OFF1; two-tailed paired t test, $t = -1.644$, $P = 0.139$ for laser ON, $t = 4.843$, $P = 0.001$ for laser OFF2) and discrimination score between the OFF1 and ON phases (**i**: $n = 9$ mice, Wilcoxon signed-rank test, $Z = -2.547$, $P = 0.011$). **j** Same experimental design as in **a** but for

SST-Cre mice. **k** Representative images showing the injection site in vHPC (left) and ACC (right). **l** AAV1 expression in vHPC (top) and co-labeling of AAV1-EGFP and Chr2-mCherry in ACC of SST-Cre mice (bottom). **m** Representative movement traces of SST-Cre mice during the social preference test. **n**–**o** Social time of SST-Cre mice in social preference test (**n**: $n = 8$ mice; two-tailed paired t test, $t = 5.238$, $P = 0.0012$ for laser OFF1; $t = -4.202$, $P = 0.004$ for laser ON; $t = 3.420$, $P = 0.011$ for laser OFF2) and the discrimination score between the OFF1 and ON phases (**o**: $n = 8$ mice, two-tailed paired t test, $t = 10.065$, $P < 0.0001$). **p**, **q** Social interaction time between Chr2 and mCherry control groups in the original zone for SST-Cre mice (**p**: $n = 8$ mice for Chr2, $n = 6$ mice for mCherry; repeated-measures ANOVA, $F_{\text{between group}} = 5.978$, $P = 0.031$, $F_{\text{within group}} = 5.444$, $P = 0.011$) and quantification of social interaction time when the laser was ON (**q**: two-tailed unpaired t -test, $t = 3.788$, $P = 0.003$). The 3D images of (**a**, **j**) were created with CEBIT/ION Digital Brain <https://www.digital-brain.cn/>. All statistical tests are two-sided. Data are presented as mean \pm SEM. * $P < 0.05$, ** $P < 0.01$, **** $P < 0.0001$. Source data are provided as a Source Data File.

Methods

Mice

All experimental procedures were approved by the Institutional Animal Care and Use Committee (IACUC-20220312) of the Fourth Military Medical University and carried out according to the “Principles of Medical Laboratory Animal Care” issued by the National Ministry of

Health in China. Adult (6–8-week-old) male PV-Cre (Jax Stock no. 017032), SST-Cre (Jax Stock no. 013044), PV-tdTomato (Jax Stock no. 027395), Ai9 (Jax Stock no. 007909), *Shank3* KO⁷ (Jax Stock no. 017688) and C57BL6 mice were used in this study. The animals were housed under a 12 h:12 h light:dark cycle (lights on at 8 AM), with food and water provided *ad libitum*. Subjects were assigned randomly, and

no mice were excluded unless they exhibited weight loss exceeding 10% during subsequent experiments or if viral injections were performed inaccurately, as confirmed by post hoc analysis of viral targeting. The researchers were blinded to the experimental groups. All mice were euthanized using a humane method in accordance with the *Principles of Medical Laboratory Animal Care*.

Surgical procedures

General procedure. Six-to-eight-week-old mice were used for stereotaxic injections. The mice were anesthetized with 1% pentobarbital sodium and placed in a stereotaxic instrument (RWD). Eye ointment and a piece of silver paper were applied to prevent corneal drying. A thermostatic heating pad (RWD) was used to keep the mouse body temperature constant during surgery. A small craniotomy hole was made using a dental drill (RWD), and injections were carried out using a microsyringe pump (KD Scientific) at a flow rate of 40 nL/min to minimize brain tissue damage.

GCaMP imaging. Fiber photometry was used to record calcium signals via a commercialized fiber photometry system. AAV2/9-CAG-FLEX-GCaMP7s (2.21E + 12 vg/mL, 240 nL/injection) was injected unilaterally into the ACC of PV-Cre or SST-Cre mice (AP: +0.73 mm; ML: -0.28 mm; DV: -1.75 mm). Three weeks later, optical fibers (2.5 mm optical density (O.D.), 0.5 numerical aperture (N.A.), 2.5 mm length) were implanted ipsilaterally. We used dental acrylic resin (Super Bond) to support the ceramic ferrule. The mice were housed individually and allowed to recover for at least one week before subsequent experiments.

Optogenetics. AAV2/9-DIO-ChR2-EYFP was injected unilaterally into the ACC of PV-Cre or SST-Cre mice (virus titer: 3.2E + 12 vg/mL, 240 nL/injection; AP: +0.73 mm; ML: -0.28 mm; DV: -1.75 mm), and optical fibers (2.5 mm O.D., 0.37 N.A., 2.0 mm length) were implanted ipsilaterally.

Fluorescence assay of pyramidal neurons regulated by interneuron activity. A mixture of AAV2/9-CaMKII-GCaMP6s (5.36E + 12 vg/mL) and AAV2/9-hSyn-DIO-ChrimsonR-mCherry (2.50E + 12 vg/mL) at 1:8 ratio (200 nL total volume) was injected unilaterally into the ACC of PV-Cre or SST-Cre mice at the same coordinates as the previous site (AP: +0.73 mm; ML: -0.28 mm; DV: -1.75 mm). Two weeks later, optical fibers (2.5 mm O.D., 0.37 N.A., 2.5 mm length) were implanted ipsilaterally.

Retrograde RV tracing of PV or SST interneuron monosynaptic inputs to the ACC. To specifically map the monosynaptic inputs to PV or SST interneurons, a mixture of AAV-EF1a-DIO-Histone-EGFP-T2A-TVA and rAAV-EF1a-DIO-oRVG (1:1 ratio, 200 nL total volume) was injected unilaterally into the ACC of PV-Cre or SST-Cre mice. The AAV helper vector and AAV-double-floxed inverted open reading frame (DIO)-RVG enabled the visualization of starter neurons and provided essential components for retrograde tracing. Three weeks later, RV-EnvA-ΔG-dsRed was injected at the same coordinates to label upstream neurons. This viral strategy ensured efficient RV generation and optimization of RV-dsRed retrograde spread⁵⁵. The density of upstream neurons was analyzed with reference to *the Mouse Brain in Stereotaxic Coordinates* (Second Edition).

Functional verification of the projection loop. To trace synaptic connections from the LPMR to PV interneurons and from the vHPC to SST interneurons in the ACC, and to confirm the functional role of these projections, a mixture of AAV_{Retro}-ChR2 (5.08E + 12 vg/mL) and AAV2/9-CAG-FLEX-GCaMP7s (2.21E + 12 vg/mL) was injected into the ACC of PV-Cre and SST-Cre mice (240 nL/injection). Optical fibers (3.0 mm length or 4.0 mm length) were implanted in the ipsilateral LPMR (AP: -1.95 mm; ML: -1.64 mm; DV: -2.52 mm) or

vHPC (AP: -3.2 mm; ML: -3.81 mm; DV: -1.57 mm) at a 15° angle. Additionally, optical fiber (2.5 mm length) was implanted ipsilaterally in the ACC. To confirm the function of these two projections in vitro, AAV2/9-hSyn-ChR2-mCherry (3.84 E + 12 vg/mL, 240 nL/injection) was injected into the LPMR or vHPC of PV-tdTomato or SST-Cre::Ai9 mice.

Specific projection regulation. To achieve trans-monosynaptic anterograde expression of Flippase (Flp) in the LPMR or vHPC, AAV1-Flp-EGFP (3.51 E + 13 vg/mL, 200 nL/injection) was injected into the LPMRs (AP: -1.95 mm; ML: -0.85 mm; DV: -3.15 mm) of PV-Cre mice, and AAV1-Flp-EGFP was injected into the vHPCs (AP: -3.2 mm; ML: -3.2 mm; DV: -2.8 mm) of SST-Cre mice. Additionally, AAV2/9-hSyn-Con-Fon-mCherry (5.56 E + 12 vg/mL, 200 nL/injection) was injected into the ACC of PV-Cre or SST-Cre mice. This approach employed Boolean logic operations by utilizing multiple recombinase systems to drive the expression of reporter genes. Through intersectional strategies, requiring the expression of all recombinases, specific cell subpopulations were targeted with greater precision⁵⁶. The optical fibers were implanted in ACC ipsilaterally. For specific regulation of MD → PV interneurons, Po → PV interneurons, MD → SST interneurons and Cl/Den → SST interneurons in the ACC, AAV1-Flp-EGFP was injected into the MD (AP: -1.0 mm; ML: -0.75 mm; DV: -3.4 mm), Po (AP: -1.95 mm; ML: -1.25 mm; DV: -3.5 mm), and Cl/Den (AP: +1.5 mm; ML: -0.85 mm; DV: -3.0 mm).

Virus intervention by taCasp3. To suppress the activity of PV or SST interneurons and observe the impact on social behavior in mice, AAV2/9-FLEX-taCasp3 (2.03E + 12 vg/mL, 240 nL/injection) was bilaterally injected into the ACC.

Virus intervention by knocking out Kcnh7. To specifically knockout *Kcnh7* on PV and SST neurons, a mixture of AAV-MECP2-DIO-Cas9 (4.79E + 13 vg/mL) and AAV-kcnh7-gRNA-hSyn-GFP (1.55E + 13 vg/mL), 240 nL total volume/injection, was injected bilaterally into the ACC of PV-Cre and SST-Cre mice.

Fiber photometry analysis

GCaMP7s fluorescence signals were detected through the optic fiber using a fiber photometry system (QAXK-FPS-SS-LED-PRO, Thinker Tech). In the home cage, the zero-point for calcium signals was defined as the moment when the nose or forelimbs of the subject mouse contacted with an unfamiliar juvenile mouse, and the fluorescence signals were analyzed over a 5 s window following the contact. As distinct social interaction events, such as genital sniffing, following, and nose or body contact (Fig. 1d), often occurred consecutively, we did not define separate zero-points for each event. In the three-chamber test, the zero-point was defined as the moment when the subject mouse approached the cage within a distance shorter than its head length, and signals were analyzed over a 5 s window following this point. The total observation time for both the home cage and three-chamber tests was 10 min. Changes in fluorescence intensity ($\Delta F/F_0$) were calculated as $\Delta F/F_0 = (F_{\text{signal}} - F_0)/F_0 - F_{\text{offset}}$, where F_0 was defined as the baseline fluorescence signal averaged over a 2 s-long control time window and F_{offset} was the system bias data recorded in the dark. F_{signal} represented the peak value of the fluorescence signal. Data analysis was performed using MATLAB-based software provided by Thinker Tech.

Behavioral tests and in vivo optogenetic manipulations

General procedure. For optical stimulation during behavioral tests, the device connection followed a previously described protocol⁷. The laser was connected to a patch cord, which was linked to a fiber-optic rotary joint, allowing free rotation of the fiber. The other end of the fiber was then connected to the ferrule mounted on the mouse's head.

Following a brief recovery period from handling, the behavioral test was initiated. In the excitatory photogenetic experiments, the test was divided into three phases: laser stimulation off, on and off (OFF1-ON-OFF2 phases). Photostimulation of PV interneurons or SST interneurons in the ACC was induced by 40 Hz light trains with 5 ms pulses generated by a 473 nm laser (IOS-465, RWD). The laser power was adjusted to approximately 5.0 mW at the tip of the fiber-optic cable. Each phase (OFF1-ON-OFF2) lasted 3 min during both the home cage and three-chamber tests.

Social interactions in the home cage. This experiment was performed as previously described⁷. One week before the experiment, the test mice underwent adaptability training, during which they were handled daily. On the test day, the mice were allowed to explore the home cage freely for 3 min (habituation) before an unfamiliar juvenile male mouse (3 weeks old) was introduced into the cage. Social interaction behaviors were defined as body sniffing, anogenital sniffing, face or nose contact, and close following (<1 cm). All behaviors were video recorded and analyzed via SMART v.3.0 software by researchers blinded to the testing conditions. The slope of the behavior in Fig. 3d was calculated as follows: the X-axis represented the social time when the laser was on (ST_{on}) minus the social time before the laser was on (ST_{off1}), divided by the total time of the test (T_T); the Y-axis represented the social time after the laser was on (ST_{off2}) minus the social time when the laser was on (ST_{on}), divided by the total time of the test (T_T). Social inhibition index: the time spent with a social object when the laser was OFF1 minus when the laser was ON, divided by the total time spent with a social object when the laser was OFF1 and ON. To observe the effect of PV or SST neuron activation on the activity of pyramidal neurons in vivo, a 589 nm laser (40 Hz, 5 mW) was used to stimulate ChrimsonR-expressing interneurons. The stimulation protocol consisted of 10 cycles of 30 s ON followed by 1 min OFF during the home cage test.

Three-chamber test. This experiment was performed as previously described⁷. The apparatus consisted of three identical chambers (30 cm × 45 cm × 20 cm) made of black perspex acrylic sheets. Two cylindrical grid cages were placed in the corners of the outer chambers, allowing free visual, olfactory, and auditory interaction between the test mouse and the caged mouse. Before the test, the test animal was placed in the chamber for 10 min to habituate and then was isolated in the middle chamber to wait for the experiment to begin. For the sociability test, a novel juvenile male mouse was placed in a wire cage in one chamber, and another empty wire cage was placed in the opposite chamber. The subject mouse was then allowed to explore all three chambers freely. For the social preference test, the second stranger juvenile male mouse was put into the other empty cage and the experimental subject mouse was allowed to explore freely in three-chambers again. The data was analyzed via SMART v.3.0 software. The discrimination score in the sociability test was calculated as the time spent in the social zone minus the time spent in the empty zone, divided by the total time spent in both zones. The discrimination score in the social preference test was calculated as the time spent in the stranger zone minus the time spent in the original zone, divided by the total time spent in both zones. The latency of the first social behavior stop was defined as the time from the start of the social interaction to the cessation of the behavior. When the subject mouse approached within a distance shorter than a mouse's head length from the cage of the object mouse, time recording and optical stimulation were initiated manually. Laser activation was defined as the zero-point, and the end of the interaction was recorded when the subject mouse turned its body away from the cage or stepped back to initiate another behavior. Each trial included only one scenario in which the subject mouse entered a social zone, engaged in social interactions, and subsequently ceased such activities.

Olfactory test. The experiment was conducted in an open field arena. Fresh urine was collected on the day of the experiment. Ten three-week-old male mice were placed in a cage lined with clean filter paper. Immediately upon urination, the urine-stained portions of the filter paper were excised. Petri dishes were prepared in advance. Collected filter paper segments were placed into one dish, which was then covered with cling film punctured with a fine array of small holes. For the saline control group, the filter paper was saturated with saline. The petri dishes with urine filter paper and saline filter paper were placed on opposite sides of the open field arena. The movement of the mice was recorded under two conditions: with the laser off and with the laser on. The time spent in each corner was analyzed using SMART v.3.0 software.

Social behavior by virus intervention. Prior to viral injection, social interaction was tested. Three weeks after the viral injection, a new round of social interaction experiments was conducted. The total observation time for each session was 10 min. The videos were analyzed via SMART v.3.0 software. Social promotion index: (social interaction time after viral intervention minus social interaction time before viral intervention) divided by (social interaction time after viral intervention plus social interaction time before viral intervention).

Immunocytochemistry

All animals were anesthetized with 1% pentobarbital sodium and perfused intracardially with 0.9% saline followed by 4% paraformaldehyde. The whole brain was then removed and placed in 30% sucrose solution for 3 days. For labeling of PV or SST interneurons, 40 μ m-thick brain tissue sections containing the ACC were placed in blocking solution for 1 h before incubation with primary antibodies against PV (rabbit, 1:100, Abcam, ab181086), SST (rat, 1:50, Millipore, MAB354), KCNH7 (rabbit, 1:50, Proteintech, 13622-1-AP), and NeuN (mouse, 1:500, Abcam, ab104224) overnight at 4 °C. For the expression of Fos, brains were collected one hour after the behavior test, and tissue sections were processed as described above. These sections were stained with anti-Fos antibody (rabbit, 1:1500, CST, #2250). The sections were incubated with the secondary antibody at a dilution of 1:800 for 4 h at room temperature. Finally, all the sections were incubated with Hoechst 33342 (Sigma) rinsed in 0.01 M PBS. Each section was mounted a microscope slide, and a cover glass was sealed on it with a mixture of 50% (v/v) glycerol in 0.01 M PBS and were then imaged with confocal (FV31S-SW, Olympus). For the RV retrograde tracing of PV or SST interneuron monosynaptic inputs, 7 days after RV-EnvA- Δ G-dsRed viral injection, the preparation of 40 μ m-thick brain tissue sections was the same as described above. All the sections were incubated with Hoechst 33342 (Sigma), rinsed with 0.01 M PBS. Each section was mounted on a microscope slide and covered with a cover glass using a mixture of 50% (v/v) glycerol in 0.01 M PBS. The slides were then scanned using a VS200 Slide Scanner (Olympus). The number of positive cells was analyzed via ImageJ software, and the area of the upstream brain region was measured via OlyVIA (Olympus). The density of cells was calculated as the number of positive cells/the area of the upstream brain region.

RNA extraction and quantitative real-time PCR

To assess the efficiency of AAV-taCasp3, real-time PCR was performed to measure the mRNA levels of *parvalbumin* and *somatostatin* as previously described⁵⁷. After the social behavior test, the mice were deeply anesthetized with isoflurane and sacrificed. The skull of each mouse was opened, and the whole brain was removed. Fresh ACC tissues were isolated from the corresponding coronal sections under a stereomicroscope. Total RNA was extracted with TRIzol reagent, and PrimeScript™ RT Master Mix (Takara) was used to reverse transcribe the total RNA (500 ng) into complementary DNA. Real-time PCR was carried out via a StepOnePlus™ Real-Time PCR instrument (Thermo)

with 2× Universal SYBR Green Fast qPCR Mix (ABclonal). The sequences of the primers used were as follows:

Gapdh-Fp: 5'-GCGAGACCCCACTAACATCAA-3',
Gapdh-Rp: 5'-GTGGTTCACACCCATCACAAA-3';
Pvalb-Fp: 5'-ATCAAGAAGGCGATAGGAGCC-3',
Pvalb-Rp: 5'-GGCCAGAAGCGTCTTTGTT-3';
Som-Fp: 5'-ACCGGGAACAGGAACTGG-3',
Som-Rp: 5'-TTGCTGGGTTCGAGTTGGC-3'.

Electrophysiological recording

General procedure. For brain slice preparation, mice were deeply anesthetized with isoflurane and transcardially perfused with ice-cold carbogenated (95% O₂, 5% CO₂) cutting solution containing 115 mM choline chloride, 2.5 mM KCl, 1.25 mM NaH₂PO₄, 0.5 mM CaCl₂, 8 mM MgCl₂, 26 mM NaHCO₃, 10 mM D-(+)-glucose, 0.1 mM L-ascorbic acid, and 0.4 mM sodium pyruvate (pH 7.4, with an osmolarity of 295–300 mOsm/L). Coronal sections (300 μm thick) containing the ACC were cut using a vibratome (7000SMZ, Campden). Then, the brain slices were incubated with carbogenated cutting solution (95% O₂, 5% CO₂) in a holding chamber at 32 °C. Afterward, the slices were incubated for 1 h at room temperature in artificial cerebral spinal fluid (ACSF; 119 mM NaCl, 2.3 mM KCl, 1.0 mM NaH₂PO₄, 26 mM NaHCO₃, 11 mM D-(+)-glucose, 1.3 mM MgCl₂, and 2.5 mM CaCl₂, pH 7.4, with an osmolarity of 295–300 mOsm/L). Following recovery, the slices were placed in the recording chamber and continuously perfused with ACSF. Recordings were obtained using an Axon Multiclamp 700B amplifier (Molecular Devices) filtered at 5 kHz and sampled at 20 kHz with a Digidata 1550B. Clampex 10.6 and Clampfit 10.7 were used for acquisition and analysis. Data were excluded if the resting membrane potential of neurons were more positive than −60 mV, if action potentials lacked overshoot, or the series resistance changed by >20%.

ChR2-evoked spike recording. To record light-induced spikes with a current clamp in PV-positive and SST-positive neurons in the ACC, patch pipettes were filled with a solution containing the following: 128 mM potassium gluconate, 10 mM Na-phosphocreatine, 10 mM HEPES, 1.1 mM EGTA, 0.5 mM Na₂GTP, and 5 mM MgATP (pH 7.3, osmolarity: 300–305 mOsm/L). In the current clamp mode of the whole-cell patch, the 5 mW intensity, 5 ms pulse width and 40 Hz 473 nm light stimulus (IOS-465, RWD) was delivered to evoke spikes during each stimulus. The Event Detection function in the Clampfit software was used to quantify the number and amplitude of the spikes.

ChR2-evoked IPSC and PPR recording. Patch pipettes were filled with a solution containing 103 mM CsCl, 12 mM CsMeSO₃, 12 mM CsOH, 12 mM methanesulfonic acid, 5 mM TEA-Cl, 10 mM HEPES, 4 mM MgATP, and 0.3 mM Na₂GTP (pH 7.3, osmolarity: 300–305 mOsm/L). The membrane potential of pyramidal neurons was held at −65 mV during laser-evoked IPSCs and PPR recordings. PV or SST interneurons were stimulated with a 5 ms pulse of 473 nm light (IOS-465, RWD). Picrotoxin (PTX, 100 μM) was added to verify the properties of the IPSCs.

Intrinsic membrane properties. To evaluate the intrinsic membrane properties of PV interneurons and SST interneurons in the ACC, whole-cell recordings were performed in current-clamp mode. The membrane potential was held at −65 mV, and spikes were elicited by incrementally increasing the current injection in 20 pA steps.

EPSC recording. Patch pipettes were filled with an internal solution containing the following 120 mM CsMeSO₃, 10 mM TEA-Cl, 5 mM NaCl, 10 mM HEPES, 4 mM MgATP, 0.3 mM Na₂GTP, 1.1 mM EGTA, and 4 mM lidocaine (pH 7.3, osmolarity: 295–300 mOsm/L). The laser intensity was adjusted to achieve a maximal response without overstimulation, and 0.5 ms pulses of blue light was applied with the cells clamped at

−65 mV. An additional 1 μM tetrodotoxin (TTX) and 100 μM 4-AP were added, followed by 20 μM NBQX, to determine whether the light-evoked PSCs were excitatory or inhibitory.

Neuronal excitability modulated by the Kv11.3 channel. To investigate the role of the Kv11.3 channel in action potentials, 1-[2-(6-methyl-2-pyridyl)ethyl]-4-(4-methylsulfonylamino)benzoyl piperidine (E-4031, Tocris), a Kv11 blocker, was added to ACSF solution. Stock solutions of E-4031 (100 μM) were prepared in DMSO and diluted in ACSF, ensuring that the final DMSO concentration did not exceed 0.1%, which had no detectable effect on the membrane potential or membrane currents.

Kv11 current recordings. For voltage-dependent K⁺ current recordings, the low-K⁺ intracellular solution was composed of 55 mM potassium methanesulfonate, 5 mM KCl, 73 mM N-methyl-D-glucamine, 5 mM NaCl, 0.5 mM EGTA, 30 mM HEPES, 4 mM MgCl₂, 4 mM MgATP and 0.4 mM Na₂GTP (pH 7.4, adjusted with HCl)⁵⁸. To record Kv11 currents from PV or SST-positive neurons in the ACC, 1 μM TTX, 20 μM NBQX, 50 μM D-AP5 and 10 μM bicuculline were added to high-K⁺ intracellular solutions (10 mM KCl and no Ca²⁺). The use of high-K⁺ extracellular and low-K⁺ intracellular solutions allowed the K⁺ currents to be recorded as large, distinct inward currents. The signals were filtered at 3 kHz and digitized at 10 kHz in experiments for Kv11 current measurements. The activation curve of the Kv11 channels was extracted by dividing the peak amplitudes of the E-4031-sensitive tail current traces at 0.5 ms after the voltage was stepped to −100 mV.

scRNA-seq

10× sample processing and cDNA library preparation. ACC tissues were rapidly dissected from the cortices of *Shank3* KO and WT mice using freshly frozen mouse brain samples. Nucleus isolation, library preparation, and sequencing were performed by Gene Denovo Biotechnology Co. Ltd. (Guangzhou, China) following the 10× Genomics (USA) guidelines. For nucleus isolation, the tissues were homogenized in ice-cold homogenization buffer (0.25 M sucrose, 5 mM CaCl₂, 3 mM MgAc₂, 10 mM Tris-HCl, pH 8.0, 0.1 mM EDTA, 1× protease inhibitor, and 1 U/μL Ribolock RNase inhibitors). The homogenates were sequentially filtered through a 70 μm cell strainer to isolate the nuclear fraction. The nuclear fraction was mixed with an equal volume of 50% iodixanol and carefully layered onto a discontinuous gradient of 30–33% iodixanol. This mixture was centrifuged at 10,000 × g for 20 min at 4 °C. After removing the myelin layer from the top of the gradient, nuclei were harvested from the interface between the 30% and 33% iodixanol layers. The isolated nuclei were resuspended in nuclei wash and resuspension buffer (0.04% bovine serum albumin, 0.2 U/μL Ribolock RNase inhibitors, 500 mM mannitol, and 0.1 mM PMSF protease inhibitor in phosphate-buffered saline) and pelleted by centrifugation at 500 × g for 5 min at 4 °C. To remove cell debris and large aggregates, the nuclei suspension was further filtered through a 40 μm cell strainer. The nuclei concentration was quantified using trypan blue exclusion staining and a hemocytometer and adjusted to 800–1200 nuclei/μL. Reverse transcription, cDNA amplification, and library preparation were performed according to the 10× Genomics protocol. Cellular suspensions were loaded onto a 10× Genomics GemCode single-cell instrument, which generated single-cell Gel Bead-in-Emulsion (GEMs). Libraries were generated and sequenced from the cDNA using Chromium Next GEM Single Cell 3' Reagent Kits v3.1.

Sequencing and cell clustering. The single-cell 3' protocol was used to produce Illumina-ready sequencing libraries. 10× Genomics Cell Ranger software (version 3.1.0) was used to convert raw BCL files to FASTQ files, perform alignment and quantify counts. Prior to quantification, Unique Molecular Identifier (UMI) sequences were corrected for sequencing errors, and valid barcodes were identified using the EmptyDrops method⁵⁹. The cell-by-gene matrices were produced via

UMI counting and cell barcodes calling. The resulting matrices were individually imported into Seurat (version 3.1.1) for downstream analysis.

Differentially expressed gene analysis. The expression levels of each gene in a given cluster were compared against those in the remaining cells using the Wilcoxon rank sum test⁶⁰.

Fluorescent in situ hybridization

The mice were deeply anesthetized with isoflurane and transcardially perfused with 0.01 M PBS (pH: 7.4), followed by 4% paraformaldehyde in 0.01 M PB. Brains were removed and fixed in 4% paraformaldehyde for 2 h and then sequentially incubated in 10%, 20%, and 30% sucrose at 4 °C until they sank. The tissues were frozen and cut into 10 µm thick coronal sections using a cryostat (Leica). RNAscope in situ hybridization was performed using the RNAscope™ Multiplex Fluorescent Reagent Kit v2 (ACD) for fixed-frozen tissue following the manufacturer's instructions. Briefly, the sections were dehydrated in sequential incubations with different concentrations of ethanol, followed by 30 min of Protease III treatment and washing in ddH₂O. Hybridization probes [*Pvalb* 421931-C1, *Sst* 404631-C1, and *Kcnh7* 1007281-C2, ACD] were incubated for 2 h at 40 °C, followed by three amplification steps, with each target incubated with a specific dye. Hoechst counterstaining and mounting were performed with antifade mounting medium. The fluorescence intensity was analyzed via ImageJ software. The total number of puncta was used to normalize mRNA expression.

Single-cell qRT-PCR

Single PV-positive or SST-positive neurons in the ACC with red fluorescence signals were aspirated using a patch clamp. Each single cell was ejected into a tube with 5 µL of 0.01 M D-PBS. Total RNA and cDNA from single neurons were isolated using a REPLI-g® WTA single-cell kit (Qiagen) according to the manufacturer's instructions. qRT-PCR was performed with SYBR® Premix Ex Taq (ABclonal) in a CFX96 Touch Real-time PCR Detection System (Bio-Rad). The primers used were as follows:

Gapdh-Fp: 5'-AGGTCGGTGTGAACGGATTTG-3',
Gapdh-Rp: 5'-TGAGACCATGTAGTTGAGGTCA-3';
Kcnh7-Fp: 5'-CCAGGAACTGGACCGATACT-3',
Kcnh7-Rp: 5'-CCAATCGCATACCAGATGCAA-3';
Kcnh6-Fp: 5'-GACGTGCTTTCCACTCTCTAC-3',
Kcnh6-Rp: 5'-GCGCTTGATTGCCTGGTC-3';
Kcnh2-Fp: 5'-GTGCTGCCTGAGTATAAGCTG-3',
Kcnh2-Rp: 5'-CCGAGTACGGTGTGAAGACT-3'.

The mean expression value of the control group was calculated. The data of the experimental group and control group were divided by this mean, and the resulting values were used for statistical analysis.

In vivo CRISPR-Cas9 genome editing

An AAV CRISPR/Cas9 approach was used to conduct the in vivo *Kcnh7* knockdown experiments. Single guide RNAs (sgRNAs) with high specificity and high efficiency were computationally identified in sgRNA libraries for genome-wide CRISPR knockout screening. Three U6-sgRNA (FE) gene fragments with the F+E tracrRNA backbone were synthesized by Integrated DNA Technologies (sequences are provided below, and spacer sequences are capitalized). These fragments were subsequently cloned and inserted into the pX552-EGFP plasmid via In-Fusion Snap assembly master mix (Takara, Catalog # 638948), resulting in the construct pX552-3xsgRNA(FE)-EGFP.

The AAV vectors were serotyped with PHP.eB coat. Briefly, the sgRNA plasmids pAdDeltaF6 (Addgene, plasmid #112867) and pUCmini-iCAP-PHP.eB (Addgene, plasmid #103005) were cotransfected into HEK293T cells using polyethylenimine (Cat. No. 23966; Polysciences). After 72 h of transfection, the cells were harvested by

centrifugation at 5000 × g for 10 min at 4 °C. The AAV vectors in the media were precipitated with 8% PEG8000 (89510-1KG-F, Sigma). The cell pellets and vectors precipitated from the media were resuspended in digestion buffer containing 500 mM NaCl, 40 mM Tris base, and 10 mM MgCl₂. Benzo nuclease (10 KU, Novoprotein) was added to the digestion buffer, and the mixture was incubated at 37 °C for 1 h. Next, the mixture was centrifuged at 2000 × g for 10 min, and the supernatant was added to a 39 mL ultracentrifuge tube with discontinuous gradients of 15%, 25%, 40%, and 60% iodixanol. Ultracentrifugation was performed at 350,000 × g for 2.5 h at 18 °C. Fractions (5 ml) from the 40% layer and 40–60% interface were collected and desalted using a 100 kDa cutoff ultrafiltration tube (15 ml, Millipore). The buffer was exchanged four times with 1× PBS containing 0.001% Pluronic F-68. AAV titers were determined via qRT-PCR using the primers for ITR. Forward primer: 5'-GGAACCCCTAGTGATGGAGTT-3'; Reverse primer: 5'-CGGCCTCAGTGAGCGA-3'.

U6-sgkcnh7-1(FE) sequence

gaggcctatttccatgattcctcatatttgcatacagatacaaggctgttagagaga-taattggaattaattgactgtaaacacaaagatattagtacaaaatacgtgacgtagaagtaa-taattcttgggtagtttgcagtttaaaattatgttttaaaatggactatca-tatgcttaccgtaactgaaagtatttcgattcttggctttatatcttggtaaaggacgaa-caccgCTGGGCAATATCATGCCTCTgtttaagagctatgctggaaacagca-tagcaagtttaataaggctagtcggtatcaacttgaaaaagtgccaccgagtcggtgct

U6-sgkcnh7-2(FE) sequence

Aaggctgggagcaggaagaggcctatttccatgattcctcatatttgcatacagata-caaggctgttagagagataattagaattaattgactgtaaacacaaagatattagtacaaa-tacgtgacgtagaaagtaataatttctgggtagtttgcagtttaaaattatgttttaaaatggac-tatcatatgcttaccgtaactgaaagtatttcgattcttggctttatatcttggtaaaggac-gaaacaccGAATATCGGGTTGACCTCTCgtttaagagctatgctggaaacagcat-agcaagtttaataaggctagtcggtatcaacttgaaaaagtgccaccgagtcggtgct

U6-sgkcnh7-3(FE) sequence

Aaggctgggagcaggaagaggcctatttccatgattcctcatatttgcatacagata-caaggctgttagagagataattagaattaattgactgtaaacacaaagatattagtacaaa-tacgtgacgtagaaagtaataatttctgggtagtttgcagtttaaaattatgttttaaaatggac-tatcatatgcttaccgtaactgaaagtatttcgattcttggctttatatcttggtaaaggac-gaaacaccGATGCCCTCCGTATGCTACAGgttttagagctagaaatagcaag-ttaaaataaggctagtcggtatcaacttgaaaaagtgccaccgagtcggtgct

Statistical analyses

All the statistical analyses were performed in Prism 9.5.1 (GraphPad Software, Inc., USA) and SPSS 21.0. The values are expressed as the means ± standard errors of the mean (SEMs). The significance of the data was tested using either an unpaired *t*-test or a two-way repeated-measures ANOVA. For datasets that were normally distributed, a two-tailed unpaired *t*-test and two-way repeated-measures ANOVA were used, followed by Tukey's multiple comparisons test. For datasets that were not normally distributed, a Kruskal-Wallis test was applied with adjustments for multiple comparisons (Supplementary Data 1). All behavioral, electrophysiological, biochemical and morphological data were collected under both experimental and control conditions. Details of the specific statistical analyses are provided in Supplementary Data 1. Statistical significance was considered when *p* < 0.05.

Reporting summary

Further information on research design is available in the Nature Portfolio Reporting Summary linked to this article.

Data availability

All data generated in this study are provided in the Source Data file. The raw scRNA-seq data have been deposited in the Genome Sequence Archive at the BIG Data Center (<http://bigd.big.ac.cn/>), Beijing Institute of Genomics (BIG), Chinese Academy of Sciences, under the accession

number CRA013264. The expression of marker genes in different clusters is shown in Supplementary Information (Supplementary Data 2). Source data are provided with this paper.

References

- Chen, P. & Hong, W. Neural circuit mechanisms of social behavior. *Neuron* **98**, 16–30 (2018).
- Moy, S. S. et al. Sociability and preference for social novelty in five inbred strains: an approach to assess autistic-like behavior in mice. *Genes Brain Behav.* **3**, 287–302 (2004).
- Jang, S. et al. Impact of the circadian nuclear receptor REV-ERB α in dorsal raphe 5-HT neurons on social interaction behavior, especially social preference. *Exp. Mol. Med.* **55**, 1806–1819 (2023).
- Tian, R. et al. Modeling SHANK3-associated autism spectrum disorder in Beagle dogs via CRISPR/Cas9 gene editing. *Mol. Psychiatry* **28**, 3739–3750 (2023).
- Ariyasiri, K. et al. Pharmacological (ethanol) and mutation (sam2 KO) induced impairment of novelty preference in zebrafish quantified using a new three-chamber social choice task. *Prog. Neuro-Psychopharmacol. Biol. Psychiatry* **88**, 53–65 (2019).
- Jabarin, R., Netser, S. & Wagner, S. Beyond the three-chamber test: toward a multimodal and objective assessment of social behavior in rodents. *Mol. Autism* **13**, 41 (2022).
- Guo, B. et al. Anterior cingulate cortex dysfunction underlies social deficits in Shank3 mutant mice. *Nat. Neurosci.* **22**, 1223–1234 (2019).
- Peça, J. et al. Shank3 mutant mice display autistic-like behaviours and striatal dysfunction. *Nature* **472**, 437–442 (2011).
- Rudebeck, P. H., Buckley, M. J., Walton, M. E. & Rushworth, M. F. A role for the macaque anterior cingulate gyrus in social valuation. *Science* **313**, 1310–1312 (2006).
- Wittmann, M. K., Lockwood, P. L. & Rushworth, M. F. S. Neural mechanisms of social cognition in primates. *Annu. Rev. Neurosci.* **41**, 99–118 (2018).
- Assaf, M. et al. Abnormal functional connectivity of default mode sub-networks in autism spectrum disorder patients. *NeuroImage* **53**, 247–256 (2010).
- Laidi, C. et al. Decreased cortical thickness in the anterior cingulate cortex in adults with autism. *J. Autism Dev. Disord.* **49**, 1402–1409 (2019).
- Riedemann, T. & Sutor, B. Cell-type-specific effects of somatostatin on synaptic transmission in the anterior cingulate cortex. *J. Neurosci.* **44**, e0598232024 (2024).
- Zhang, C. et al. Dynamics of a disinhibitory prefrontal microcircuit in controlling social competition. *Neuron* **110**, 516–531.e516 (2022).
- Jiang, C. et al. Morphine coordinates SST and PV interneurons in the prelimbic cortex to disinhibit pyramidal neurons and enhance reward. *Mol. Psychiatry* **26**, 1178–1193 (2021).
- Udakis, M., Pedrosa, V., Chamberlain, S. E. L., Clopath, C. & Mellor, J. R. Interneuron-specific plasticity at parvalbumin and somatostatin inhibitory synapses onto CA1 pyramidal neurons shapes hippocampal output. *Nat. Commun.* **11**, 4395 (2020).
- Royer, S. et al. Control of timing, rate and bursts of hippocampal place cells by dendritic and somatic inhibition. *Nat. Neurosci.* **15**, 769–775 (2012).
- Tremblay, R., Lee, S. & Rudy, B. GABAergic interneurons in the neocortex: from cellular properties to circuits. *Neuron* **91**, 260–292 (2016).
- Bhat, S., Acharya, U. R., Adeli, H., Bairy, G. M. & Adeli, A. Autism: cause factors, early diagnosis and therapies. *Rev. Neurosci.* **25**, 841–850 (2014).
- Lai, M. C., Lombardo, M. V. & Baron-Cohen, S. Autism. *Lancet* **383**, 896–910 (2014).
- Pelphrey, K. A., Shultz, S., Hudac, C. M. & Vander Wyk, B. C. Research review: constraining heterogeneity: the social brain and its development in autism spectrum disorder. *J. Child Psychol. Psychiatry Allied Discip.* **52**, 631–644 (2011).
- Griswold, A. J. et al. Targeted massively parallel sequencing of autism spectrum disorder-associated genes in a case control cohort reveals rare loss-of-function risk variants. *Mol. Autism* **6**, 43 (2015).
- Yildirim, C. & Bal, R. ERG channels regulate excitability in stellate and bushy cells of mice ventral cochlear nucleus. *J. Membr. Biol.* **251**, 711–722 (2018).
- Xu, H. et al. A disinhibitory microcircuit mediates conditioned social fear in the prefrontal cortex. *Neuron* **102**, 668–682.e665 (2019).
- Wang, H. et al. A molecularly defined amygdala-independent tetra-synaptic forebrain-to-hindbrain pathway for odor-driven innate fear and anxiety. *Nat. Neurosci.* **27**, 514–526 (2024).
- Iaccarino, H. F. et al. Gamma frequency entrainment attenuates amyloid load and modifies microglia. *Nature* **540**, 230–235 (2016).
- Monteiro, P. & Feng, G. SHANK proteins: roles at the synapse and in autism spectrum disorder. *Nat. Rev. Neurosci.* **18**, 147–157 (2017).
- Wang, X. et al. Synaptic dysfunction and abnormal behaviors in mice lacking major isoforms of Shank3. *Hum. Mol. Genet.* **20**, 3093–3108 (2011).
- Speed, H. E. et al. Autism-associated insertion mutation (InsG) of Shank3 Exon 21 causes impaired synaptic transmission and behavioral deficits. *J. Neurosci.* **35**, 9648–9665 (2015).
- Jaramillo, T. C. et al. Altered striatal synaptic function and abnormal behaviour in Shank3 Exon4-9 deletion mouse model of autism. *Autism Res.* **9**, 350–375 (2016).
- Mei, Y. et al. Adult restoration of Shank3 expression rescues selective autistic-like phenotypes. *Nature* **530**, 481–484 (2016).
- Wang, X. et al. Altered mGluR5-Homer scaffolds and corticostriatal connectivity in a Shank3 complete knockout model of autism. *Nat. Commun.* **7**, 11459 (2016).
- Zhou, Y. et al. Mice with Shank3 mutations associated with ASD and Schizophrenia display both shared and distinct defects. *Neuron* **89**, 147–162 (2016).
- Butler, A., Hoffman, P., Smibert, P., Papalexi, E. & Satija, R. Integrating single-cell transcriptomic data across different conditions, technologies, and species. *Nat. Biotechnol.* **36**, 411–420 (2018).
- Aran, D. et al. Reference-based analysis of lung single-cell sequencing reveals a transitional profibrotic macrophage. *Nat. Immunol.* **20**, 163–172 (2019).
- Callaway, E. M. & Luo, L. Monosynaptic circuit tracing with glycoprotein-deleted rabies viruses. *J. Neurosci.* **35**, 8979–8985 (2015).
- Luo, L. Architectures of neuronal circuits. *Science* **373**, eabg7285 (2021).
- Kepecs, A. & Fishell, G. Interneuron cell types are fit to function. *Nature* **505**, 318–326 (2014).
- Bertoni, A. et al. Oxytocin administration in neonates shapes hippocampal circuitry and restores social behavior in a mouse model of autism. *Mol. Psychiatry* **26**, 7582–7595 (2021).
- Weible, A. P., Rowland, D. C., Pang, R. & Kentros, C. Neural correlates of novel object and novel location recognition behavior in the mouse anterior cingulate cortex. *J. Neurophysiol.* **102**, 2055–2068 (2009).
- Kahnau, P. et al. A systematic review of the development and application of home cage monitoring in laboratory mice and rats. *BMC Biol.* **21**, 256 (2023).
- Klausberger, T. & Somogyi, P. Neuronal diversity and temporal dynamics: the unity of hippocampal circuit operations. *Science* **321**, 53–57 (2008).
- Katona, L. et al. Sleep and movement differentiates actions of two types of somatostatin-expressing GABAergic interneuron in rat hippocampus. *Neuron* **82**, 872–886 (2014).

44. Conte, W. L., Kamishina, H., Corwin, J. V. & Reep, R. L. Topography in the projections of lateral posterior thalamus with cingulate and medial agranular cortex in relation to circuitry for directed attention and neglect. *Brain Res.* **1240**, 87–95 (2008).
45. Hu, Y. et al. A translational study on looming-evoked defensive response and the underlying subcortical pathway in autism. *Sci. Rep.* **7**, 14755 (2017).
46. Green, S. A., Hernandez, L., Bookheimer, S. Y. & Dapretto, M. Reduced modulation of thalamocortical connectivity during exposure to sensory stimuli in ASD. *Autism Res.* **10**, 801–809 (2017).
47. Montagrin, A., Saiote, C. & Schiller, D. The social hippocampus. *Hippocampus* **28**, 672–679 (2018).
48. Okuyama, T., Kitamura, T., Roy, D. S., Itohara, S. & Tonegawa, S. Ventral CA1 neurons store social memory. *Science* **353**, 1536–1541 (2016).
49. Yamawaki, N. et al. Long-range inhibitory intersection of a retrosplenial thalamocortical circuit by apical tuft-targeting CA1 neurons. *Nat. Neurosci.* **22**, 618–626 (2019).
50. Utashiro, N. et al. Long-range inhibition from prelimbic to cingulate areas of the medial prefrontal cortex enhances network activity and response execution. *Nat. Commun.* **15**, 5772 (2024).
51. Leow, Y. N. et al. Brain-wide mapping of inputs to the mouse lateral posterior (LP/Pulvinar) thalamus-anterior cingulate cortex network. *J. Comp. Neurol.* **530**, 1992–2013 (2022).
52. Sharma, V. et al. eIF2 α controls memory consolidation via excitatory and somatostatin neurons. *Nature* **586**, 412–416 (2020).
53. Ito-Ishida, A., Ure, K., Chen, H., Swann, J. W. & Zoghbi, H. Y. Loss of MeCP2 in parvalbumin- and somatostatin-expressing neurons in mice leads to distinct rett syndrome-like phenotypes. *Neuron* **88**, 651–658 (2015).
54. Chen, Q. et al. Dysfunction of cortical GABAergic neurons leads to sensory hyper-reactivity in a Shank3 mouse model of ASD. *Nat. Neurosci.* **23**, 520–532 (2020).
55. Åhrlund-Richter, S. et al. A whole-brain atlas of monosynaptic input targeting four different cell types in the medial prefrontal cortex of the mouse. *Nat. Neurosci.* **22**, 657–668 (2019).
56. Ubina, T. et al. ExBoX - a simple Boolean exclusion strategy to drive expression in neurons. *J. Cell Sci.* **134**, jcs257212 (2021).
57. Qi, C. et al. Excitatory and inhibitory synaptic imbalance caused by brain-derived neurotrophic factor deficits during development in a valproic acid mouse model of autism. *Front. Mol. Neurosci.* **15**, 860275 (2022).
58. Matsuoka, T. et al. Kv11 (ether-à-go-go-related gene) voltage-dependent K(+) channels promote resonance and oscillation of subthreshold membrane potentials. *J. Physiol.* **599**, 547–569 (2021).
59. Lun, A. T. L. et al. EmptyDrops: distinguishing cells from empty droplets in droplet-based single-cell RNA sequencing data. *Genome Biol.* **20**, 63 (2019).
60. Camp, J. G. et al. Multilineage communication regulates human liver bud development from pluripotency. *Nature* **546**, 533–538 (2017).

Acknowledgements

We thank Prof. Guoping Feng (Massachusetts Institute of Technology) for his suggestions and conversation. This study was supported by the Natural Science Foundation of China (32394032 to S.W.), the Science and Technology Innovation 2030 Project of China (2021ZD0201005 to S.W.), the Natural Science Foundation of China (82221001 to S.W., 82271577, 82071536 to W.W., 82271578 to Q.C.), the Shaanxi Provincial Key Research and Development Program (2020ZDLSF01–09 to S.W.),

the Shaanxi Provincial Innovation Chain Project of Key Industries (2023-ZDLSF-47 to W.W.), the Shaanxi Province Key Research and Development Plan (2024SF-YBXM-033, C.Q.), the Joint Founding Project of Innovation Research Institute, Xijing Hospital (LHJJ24JH05 to W.W.), the Shanghai Pujiang Program (22PJ1415500 to Q.C.), the Zhongshan Municipal Bureau of Science and Technology Grant (CXTD2022013 to Q.C.), Guangdong Province High-level Innovative Research Institute project (2021B0909050003, Q.C.), and Innovation Team Accredited by Shaanxi Science and Technology (2022TD-49 to W.W.). We thank Analysis & Testing Laboratory for Life Sciences and Medicine of Fourth Military Medical University for their assistance with behavioral test, fiber photometry experiments, and in vivo optogenetic experiments. We thank American Journal Experts for language editing (Certificate NO: 9183-20FC-2A00-204D-DD6P).

Author contributions

C.Q., Q.C., W.W. and S.W. designed the experiments. C.Q., W.S., H.M., E.H., J.G., M.D., A.C., W.Y. and Q.X. performed the experiments and analyzed the data. C.Q., W.S., H.M., Q.C., W.W. and S.W. interpreted the data. C.Q., Q.C., W.W. and S.W. wrote the paper.

Competing interests

The authors declare no competing interests.

Additional information

Supplementary information The online version contains supplementary material available at <https://doi.org/10.1038/s41467-025-59473-z>.

Correspondence and requests for materials should be addressed to Wenting Wang, Qian Chen or Shengxi Wu.

Peer review information *Nature Communications* thanks the anonymous reviewers for their contribution to the peer review of this work. A peer review file is available.

Reprints and permissions information is available at <http://www.nature.com/reprints>

Publisher's note Springer Nature remains neutral with regard to jurisdictional claims in published maps and institutional affiliations.

Open Access This article is licensed under a Creative Commons Attribution-NonCommercial-NoDerivatives 4.0 International License, which permits any non-commercial use, sharing, distribution and reproduction in any medium or format, as long as you give appropriate credit to the original author(s) and the source, provide a link to the Creative Commons licence, and indicate if you modified the licensed material. You do not have permission under this licence to share adapted material derived from this article or parts of it. The images or other third party material in this article are included in the article's Creative Commons licence, unless indicated otherwise in a credit line to the material. If material is not included in the article's Creative Commons licence and your intended use is not permitted by statutory regulation or exceeds the permitted use, you will need to obtain permission directly from the copyright holder. To view a copy of this licence, visit <http://creativecommons.org/licenses/by-nc-nd/4.0/>.

© The Author(s) 2025